Fifteen shades of green: The evolution of *Bufotes* toads revisited

ChristopheDufresnes[ab1], Glib Mazepa[cd1], Daniel Jablonski[e], Ricardo Caliari Oliveira[f], Tom Wenseleers[f], Dmytro A. Shabanov[g], Markus Auer[h], Raffael Ernst[h], Claudia Koch[i], Héctor E. Ramírez-Chaves[j,k], Kevin Patrick Mulder[l,m,n], Evgeniy Simonov[o,p], Arthur Tiutenko[q], Dmytro Kryvokhyzha[r], Paul L. Wennekes[s], Oleksandr I. Zinenko[g,t], Oleksiy V. Korshunov[g], Awadh M.Al-Johany[u], Evgeniy A.Peregontsev[v], Rafaqat Masroor[w], Caroline Betto-Colliard[c], Mathieu Denoël[x], Leo J. Borkin[y], Dmitriy V. Skorinov[z], Roza A. Pasynkova[z], Lyudmila F. Mazanaeva[aa], Juriy M. Rosanov[z], Sylvain Dubey[b,c,ab], Spartak Litvinchuk[z,aa]

[a]*Laboratory for Conservation Biology, Biophore Building, University of Lausanne, 1015 Lausanne, Switzerland*
[b]*Hintermann & Weber, Avenue des Alpes 25, 1820 Montreux, Switzerland*
[c]*Department of Ecology and Evolution, Biophore Building, University of Lausanne, 1015 Lausanne, Switzerland*
[d]*Department of Ecology and Genetics, Evolutionary Biology, Norbyvägen 18D, 75236 Uppsala, Sweden*
[e]*Department of Zoology, Comenius University in Bratislava, Mlynská dolina, Ilkovičova 6, 842 15 Bratislava, Slovakia*
[f]*Laboratory of Socioecology and Social Evolution, Zoological Institute, KU Leuven, Naamsestraat 59, 3000 Leuven, Belgium*
[g]*Department of Zoology and Animal Ecology, V. N. Karazin Kharkiv National University, Svobody Square 4, Kharkiv 61022, Ukraine*
[h]*Museum of Zoology, Senckenberg Natural History Collections Dresden, Königsbrücker Landstr. 159, D-01109 Dresden, Germany*
[i]*Zoologisches Forschungsmuseum Alexander Koenig (Leibniz-Institut für Biodiversität der Tiere), Bonn, Germany*
[j]*Facultad de Ciencias Exactas y Naturales, Departamento de Ciencias Biológicas, Universidad de Caldas, Calle 65 # 26-10, Manizales, Caldas, Colombia*
[k]*Centro de Museos, Museo de Historia Natural, Universidad de Caldas, Calle 65 # 26-10, Manizales, Caldas, Colombia*
[l]*CIBIO/InBIO, Centro de Investigação em Biodiversidade e Recursos Genéticos da Universidade do Porto, Campus Agrário de Vairão, 4485-661 Vairão, Portugal*
[m]*Center for Conservation Genomics, Smithsonian Conservation Biology Institute, National Zoological Park, 3001 Connecticut Ave NW, Washington, DC 20008, USA*
[n]*Department of Vertebrate Zoology, National Museum of Natural History, Smithsonian Institution, 10th St. & Constitution Ave. NW, Washington, DC 20560, USA*
[o]*Institute of Systematics and Ecology of Animals of the Siberian Branch of the Russian Academy of Sciences, Research Group of Physiology and Genetics of Hydrobionts, Novosibirsk 630091, Russia*
[p]*Federal Research Center "Krasnoyarsk Science Center of the Siberian Branch of the Russian Academy of Sciences", Laboratory of Genomic Research and Biotechnology, Krasnoyarsk 660036, Russia*
[q]*University of Erlangen-Nuremberg, Schlossplatz 6, D91054 Erlangen, Germany*
[r]*Department of Medical Biochemistry and Microbiology, Uppsala University, Uppsala Biomedicinska Centrum (BMC), Box 582, 75123 Uppsala, Sweden*
[s]*Plant Systemics and Evolution, School of Biological Sciences, University of Reading, Philip Lyle Building 208, Pepper Ln, RG6 6LA Reading, United Kingdom*
[t]*The Museum of Nature at V. N. Karazin Kharkiv National University, Trinkler St. 8, Kharkiv 61058, Ukraine*
[u]*Department of Zoology, King Saud University, Riyadh 11451, Saudi Arabia*
[v]*Zoocomplex MChJ, Gagarin Vil. 14, 100149 Sergeli District, Tashkent City, Uzbekistan*
[w]*Pakistan Museum of Natural History, Garden Avenue, Shakarparian, Islamabad 44000, Pakistan*
[x]*Laboratory of Fish and Amphibian Ethology, Behavioural Biology Group, Freshwater and OCeanic science Unit of reSearch (FOCUS), University of Liège, Liège, Belgium*
[y]*Department of Herpetology, Zoological Institute, Russian Academy of Sciences, 199034 St. Petersburg, Russia*
[z]*Institute of Cytology, Russian Academy of Sciences, Saint Petersburg, Russia*
[aa]*Dagestan State University, Makhachkala, Russia*
[ab]*Agrosustain SA, Route de Duillier 50, 1260 Nyon, Switzerland*

Highlights

• 15 *Bufotes* species dissected by genomics and multiple genetic/biometric datasets.
• Widespread mitochondrial replacements and the super-cryptic species concept.
• Diverse but asymmetric origins of allopolyploid hybrid species.
• A discontinuous speciation continuum across 10 pairs of hybridizing lineages.
• Major taxonomic revisions, including the descriptions of two new species.

Abstract

The radiation of Palearctic green toads (*Bufotes*) holds great potential to evaluate the role of hybridization in phylogeography at multiple stages along the speciation continuum. With fifteen species representing three ploidy levels, this model system is particularly attractive to examine the causes and consequences of allopolyploidization, a prevalent yet enigmatic pathway towards hybrid speciation. Despite substantial efforts, the evolutionary history of this species complex remains largely blurred by the lack of consistency among the corresponding literature. To get a fresh, comprehensive view on *Bufotes* phylogeography, here we combined genome-wide multilocus analyses (RAD-seq) with an extensive compilation of mitochondrial, genome size, niche modelling, distribution and phenotypic (bioacoustics, morphometrics, toxin composition) datasets, representing hundreds of populations throughout Eurasia. We provide a fully resolved nuclear phylogeny for *Bufotes* and highlight exceptional cyto-nuclear discordances characteristic of complete mtDNA replacement (in 20% of species), mitochondrial surfing during post-glacial expansions, and the formation of homoploid hybrid populations. Moreover, we traced the origin of several allopolyploids down to species level, showing that all were exclusively fathered by the West Himalayan *B. latastii* but mothered by several diploid forms inhabiting Central Asian lowlands, an asymmetry consistent with hypotheses on mate choice and Dobzhansky-Muller incompatibilities. Their intermediate call phenotypes potentially allowed for rapid reproductive isolation, while toxin compositions converged towards the ecologically-closest parent. Across the radiation, we pinpoint a stepwise progression of reproductive isolation through time, with a threshold below which hybridizability is irrespective of divergence (<6My), above which species barely admix and eventually evolve different mating calls (6–10My), or can successfully cross-breed through allopolyploidization (>15My). Finally, we clarified the taxonomy of *Bufotes* (including genetic analyses of type series) and formally described two new species, *B. cypriensis* sp. nov. (endemic to Cyprus) and *B. perrini* sp. nov. (endemic to Central Asia). Embracing the genomic age, our framework marks the advent of a new exciting era for evolutionary research in these iconic amphibians.

1. Introduction

Hybridization is one major driver of the hidden diversity found in cryptic radiations, with a myriad of fascinating outcomes such as lineage fusion (Garrick et al., 2019), hotspots of genetic diversity (Canestrelli et al., 2014), reinforcement (Pfennig, 2016), adaptive introgression (Racimo et al., 2015), and the spontaneous formation of novel taxa (Ottenburghs, 2018). As a consequence, past and present hybridization are important sources of ambiguities in

phylogeography, i.e. when gene and species trees end up telling radically different stories (e.g. Shaw, 2002, Zink and Barrowclough, 2008).

Cyto-nuclear discordances bear the hallmark of past episodes of gene flow between closely-related clades (Bonnet et al., 2017), mediated by selective (asymmetric backcrossing, e.g. Chan and Levin, 2005; positive selection, e.g. Jin et al., 2018) and demographic factors (sex-biased dispersal, e.g. Dai et al., 2013; drift, e.g. Currat et al., 2008). As shown theoretically (Hallatschek and Nelson, 2008) and empirically (Berthier et al., 2007), local hybridization events can promote rampant mitochondrial introgression during range expansions, sometimes up to the complete replacement of a species' mtDNA (e.g. Zieliński et al., 2013). In fact, such remarkable situations may be more common than previously assumed, especially in fast-dispersing and male-heterogametic organisms where Haldane's rule posits that females are the fittest hybrids (Toews and Brelsford, 2012). This implies that cryptic evolutionary entities, hidden by the absence of both eco-morphological and mitochondrial differentiation, may remain unknown to science, even in well-studied biogeographic regions.

Hybrid speciation can be viewed as a special case of cyto-nuclear discordance. This phenomenon is rare among animals, given the challenge to produce reproductively isolated hybrid lineages that can escape close competition with their parental taxa (Chapman and Burke, 2007, Mallet et al., 2015). On the one hand, parental species should be sufficiently diverged so hybrids resist genetic introgression and assimilation, while benefiting from novel adaptive combinations (Wetherington et al., 1987). On the other hand, their genomes should remain compatible enough to succesfully complete gametogenesis and overcome Dobzhansky-Muller incompatibilities, so some fertility and viability are maintained (Turelli and Orr, 2000). Polyploidization offers a pathway to circumvent these issues: disturbed meiosis in F1-hybrids increases the chance to produce unreduced 2n gametes, which develop into polyploids upon fertilization (Chapman and Burke, 2007). Strongly differing by genome content, allopolyploids may then become independent sexually-reproducing entities, and occupy novel ecological spaces (Buerkle et al., 2003). Yet, given the numerous constraints to bypass, hybrid taxa are expected to have complex ancestries, further affected by their phylogeography and those of their ancestors. Tracing their origin offers windows to characterize the genomic plasticity underlying hybrid speciation, but it requires an accurate knowledge of their evolutionary history.

A first step of paramount importance to grasp these far-reaching consequences of hybridization is to contrast mitochondrial and nuclear divergences under comprehensive phylogeographic frameworks. Cyto-nuclear discordances are particularly informative as they hold records of the last episodes of hybridization (Weisrock et al., 2005). These aspects are also pivotal for integrative species delimitation (Padial et al., 2010), i.e. to support specific *vs* subspecific levels (based on the amount of genetic divergence and hybridizability), to accurately determine range limits, and to clarify the nature of taxonomically relevant populations.

Yet, the vast majority of phylogeographic work primarily relies on mitochondrial markers, traditionally combined with a few nuclear sequences such as polymorphic introns. Their lack of phylogenetic resolution and ancestral variation may be confounded with interspecific admixture (Degnan and Rosenberg, 2009), or even mimic nuclear divergence (e.g. Dubey et al., 2019). The advent of affordable high-throughput sequencing approaches like RAD-sequencing (RAD-seq) now allows to overcome these limits and incorporate genome-wide analyses of admixture across diverged groups of taxa (Coates et al., 2018), notably to clarify their taxonomy (e.g. Dufresnes et al., 2018b, Dufresnes et al., 2019b, Dufresnes et al., 2019a). This exciting

new era opens unprecedented opportunities to dissect the complex evolutionary history of species groups that are prone to hybridization.

Eurasian green toads (*Bufotes*) offer an exceptional framework to examine many effects of hybridization on phylogeography and speciation. This rich radiation is represented by two ancient clades of diploid toads (Stöck et al., 2006), here referred to as the *B. latastii* group, i.e. three identified taxa restricted to Iran, Iraq, Pakistan and the Indian Himalayas, and the *B. viridis* group i.e. seven identified taxa which diversified around the Mediterranean Basin and the Middle East. Independent lineages from these two groups interbred and generated at least six described triploid and tetraploid hybrid forms inhabiting Central Asia (Stöck et al., 2001a, Stöck et al., 2006, Litvinchuk et al., 2012, Betto-Colliard et al., 2018). In parallel, green toads also remain a model for allopatric speciation: several islands host endemic lineages (e.g. Sicily, Stöck et al., 2008; in the Aegean, Dufresnes et al., 2018a) and continental taxa meet across hybrid zones reflecting different stages of the speciation continuum (Colliard et al., 2010, Dufresnes et al., 2014). Ecologically-tolerant, fast dispersing, and frequently hybridizing at range margins, these species could be susceptible to range-wide admixture and cyto-nuclear discordances that may blur their phylogeographic history. For instance, the Iranian *B. luristanicus* (from the *B. latastii* group), exhibits a mtDNA that branches to the *B. viridis* group, indicating ancient hybridization events (Stöck et al., 2006, Betto-Colliard et al., 2018).

Despite great research potential, the evolution of *Bufotes* remains largely enigmatic. Stöck et al. (2006) provided an initial mitochondrial account, progressively complemented by regional studies that independently applied various measures of nuclear variation, e.g. genome size (e.g. Litvinchuk et al., 2011), microsatellites (Colliard et al., 2010, Dufresnes et al., 2014, Dufresnes et al., 2018a, Dufresnes et al., 2018b) or intron sequences (Stöck et al., 2008, Dufresnes et al., 2014, Dufresnes et al., 2018a, Dufresnes et al., 2018b). While lacking consistency, these nuclear studies also overlooked important biogeographic regions such as the Middle East and Central Asia, two cradles of biodiversity for herpetofauna. Recently, Betto-Colliard et al. (2018) published the first nuclear phylogeny of the entire radiation (based on six short introns), but the limited sampling, weakly-supported topologies and questionable molecular clock (see Section 2.1.5 below) provided little new insights into the nuclear evolution of *Bufotes* and the origin of hybrid species.

Given these shortcomings, an integrative, fine-scale account of the diversity and distribution of Eurasian green toads across their entire ranges is timely needed. Here, we present such account, combining multilocus genomic analyses of RAD-seq loci with an extensive compilation of mitochondrial, genome-size and phenotypic data, complemented by species distribution modelling. Beyond refining phylogenetic relationships, divergence times, range limits and nomenclature of taxa, we specifically aimed at contrasting patterns of mitochondrial *vs* nuclear genetic variation to (i) unravel cyto-nuclear discordances, (ii) assess the genetic diversity of remote biogeographic regions, and (iii) document the origin of hybrid species. Our integrative framework clarifies the evolution of the *Bufotes* complex and led to several taxonomic changes, implemented herein and detailed in a dedicated section (Section 4.3).

2. Methods

2.1. Genetic analyses

2.1.1. DNA sampling

A total of 356 green toad samples representing all recognized taxa except one (the triploid *B. zugmayeri*) were collected in the field or gathered from various collections, namely: ZISP (Zoological Institute, Russian Academy of Sciences, St. Petersburg), BEV (CEFE – EPHE collection of the Biogeography and Ecology of the Vertebrates team in Montpellier), MTD (Museum für Tierkunde, Dresden), and KUMN (Museum of Nature, V. N. Karazin Kharkiv National University, Kharkiv). Samples consisted of buccal cells, blood tissues and toe clips (live adults), muscle pieces (museum specimens and road kills), and tail tips (tadpoles), preserved in 70–96% ethanol and/or at −20 °C. Detailed locality information can be found in Table S1. DNA was extracted using the Qiagen DNeasy kit or the BioSprint Robotic workstation.

2.1.2. RAD-seq data

One genomic library was prepared according to the double digest RAD (ddRAD) protocol detailed in Brelsford et al. (2016). Briefly, it consists of a restriction enzyme digest, ligation of individual barcodes, purification, PCR amplification and pooling of the ligated fragments, size-selection (400–500 bp) on gel electrophoresis, and final purification. The original protocol was followed, using enzymes *SbfI* and *MspI*.

A total of 168 individuals, representative of all available taxa and regions, were initially processed, but only 148 were kept in the final library, due to the poor yield of 20 samples. The final multiplexed library was sequenced on two lanes (single-end 125) on an Illumina Hi-Seq 2500 at the Lausanne Genomic Technologies Facility (LGTF). Raw reads were quality checked with FastQC v.0.10.1 and bioinformatically processed with STACKS 1.48 (Catchen et al., 2013), which consists of demultiplexing (module *process_radtags*), construction and cataloging of RAD loci (modules *ustacks*, *cstacks* and *sstacks*), and SNP calling (module *populations*). To this end, we applied the *denovo.pl* pipeline, using the default stacking parameters (*–M* 2, *–m* 3 and *–n* 2), which provided an appropriate balance between data quantity and quality. We then flagged 12 individuals that featured high rates of missing data (using a custom python script available at: https://github.com/DanJeffries/RADweek/blob/master/code/Summary_plotter.py), and thus retained a total of 136 individuals for the genetic analyses, representing 82 populations from 13 known taxa (Table S1).

Several datasets were generated for the purposes of our study and we optimized the filtering parameters to obtain a good ratio of the amount of loci over missing data, while accounting for paralog overmerging (*–min_maf* 0.05 and *–max_obs_het* 0.75). These included: (i) a matrix of 615 SNPs for all 136 individuals, considering loci genotyped in at least 80 populations (*–p* 80), and in at least 80% of samples per population (*–r* 0.8); (ii) a matrix of 1432 SNPs for 42 populations from the closely-related *B. sitibundus*, *B. viridis* and *B. balearicus*, free of missing data (*–p* 42, *–r* 1.0); (iii) a matrix of 433 SNPs for 37 populations of parental and hybrid species from Central Asia, free of missing data (*–p* 37, *–r* 1.0); (iv) a sequence alignment of ~ 45 kb (378 concatenated RAD tags) for 36 samples representative of the diploid species, and bearing no traces of admixture (see Section 3.1.1 and Table S1), free of missing data (*–p* 36, *–r* 1.0).

2.1.3. Mitochondrial data

In order to provide a range-wide overview of the distributions of *Bufotes* mitochondrial lineages, we combined newly generated mitochondrial sequences with data from the literature. First, we amplified and sequenced ~900 bp of the hypervariable mitochondrial control region (CR) in 134 individuals using primers CytbA-L (5′–GAATYGGRGGWCAACCAGTAGAAGACCC–3′) and ControlB-H (5′–GTCCATTGGAGGTTAAGATC TACCA–3′). Second, we barcoded 182 samples with ~600 bp of the mitochondrial 16S gene with primers 16SA (5′–CGCCTGTTTATCAAAAACAT–3′) and 16SB (5′–CCCGTCTGAACTCAGATCACG–3′). All PCRs were carried out in 25 µL reactions containing 3 µL of template DNA, 12.5 µL of nanopure water, 7.5 µL of multiplex master mix (Qiagen, containing buffer, dNTPs and hot-start polymerase), 1 µL of each primer (10 µM), and using the following conditions: 95 °C for 15′, 35 cycles of 94 °C for 30″, 53 °C for 45″ and 72 °C for 1′; 72 °C for 5′. Third, we harvested GenBank CR and 16S data originating from 22 studies (Table S2), considering records with geographic information. Altogether, the main mitochondrial lineages could be mapped across 636 localities.

2.1.4. Population genomic analyses

We first analyzed our matrix of 615 SNPs from 136 individuals using a Principal Component Analysis (PCA) on individual allele frequency, with the R packages *ade4* (Dray and Dufour, 2007) and *adegenet* (Jombart, 2008). Second, Bayesian assignment to clusters was performed with STRUCTURE (Pritchard et al., 2000), including three replicates for $K = 1–11$, each consisting of 100,000 iterations after 10,000 of burnin. We similarly ran STRUCTURE on the E-Mediterranean (1,432 SNPs) and Asian (433 SNPs) datasets. In each case, intra- and inter-K variance in likelihood was assessed by STRUCTURE HARVESTER (Earl and von Holdt, 2012), and we reported the solutions for K values upon which the likelihood had reached a plateau.

2.1.5. Phylogenetic analyses

Phylogenetic analyses were performed in the BEAST environment v. 2.4.8 (Bouckaert et al., 2014). First, for RAD data (~45 kb alignment of 36 samples representing all the diploid species), we applied a GTR + G substitution model (suggested by bModelTest, Bouckaert and Drummond, 2017), a relaxed lognormal clock and a birth–death tree model. We set up a molecular clock independent of published species ages (e.g. Stöck et al., 2006, Stöck et al., 2008, Dufresnes et al., 2014, Dufresnes et al., 2018a, Dufresnes et al., 2018b, Betto-Colliard et al., 2018), which all primarily rely on the initial mitochondrial estimates obtained by Stöck et al., 2006, Stöck et al., 2008. The latter were inferred from mitochondrial substitution rates taken from the anuran literature and we consider doubtful some of the results subsequently obtained. For instance, the calibration of the split between the North-African *B. boulengeri* and European taxa (2.5 Mya in Stöck et al., 2008, Betto-Colliard et al., 2018) is much younger than the Messinian or Miocene origin of many North-African amphibians (Ehl et al., 2019 and references therein). Moreover the root age, i.e. the split between the *B. viridis* and *B. latastii* groups, is unrealistically young (~6 Mya in Betto-Colliard et al., 2018) given that several species of these two clades persist in sympatry without gene flow (see Section 3.1.1); all the other ~6 My old amphibians we are aware of form parapatric boundaries mediated by hybrid zones (e.g. Dufresnes et al., 2015, Dufresnes et al., 2019b, Vences et al., 2014). Instead, we dated our tree according to the fossil record as registered in the fosFARbase database

(http://www.wahre-staerke.com/), and mapped in Fig. S1. Since *Bufotes* fossils are widely found as early as the lower Miocene (15–19 Mya), we assumed the radiation to be at least this old, and used a gamma-distributed prior with $\alpha = 2.0$, $\beta = 1.0$ and an offset of 15.0 Mya (broadly covering the 15–20 Mya epoch) for the tree root. Preliminary analyses based on these settings were consistent with a potential Messinian origin for the nuclear divergence of Cyprian populations (95% HDP: 9.8–4.2 Mya, see Section 3.1.1). In the final analyses, we fixed this node age to the end of the Messinian Salinity Crisis (~5.33 Mya) as a second calibration point, with a normally-distributed prior of mean = 5.33 and $\sigma = 0.1$.

To reconstruct the mitochondrial phylogeny, we analyzed 290 unique CR haplotypes identified among 882 sequences (865 bp manually aligned), available from our study and GenBank. We applied a HKY + G substitution model (bModelTest; see also Stöck et al., 2006), a relaxed lognormal clock and a birth-death tree model. As for nuclear data, we used a gamma-distributed prior for the tree root with $\alpha = 2.0$, $\beta = 1.0$ and an offset of 15.0 Mya. In the absence of a Cyprian mitochondrial divergence and given unresolved relationships between European and Asian diploid lineages (see Section 3.1.2), we opted for their most recent common ancestor as a second calibration point, using our nuclear estimation (6.9 Mya, with 95% HPD = 5.8–8.3 Mya; see Results), which translated into a normally-distributed prior of mean = 6.9 and $\sigma = 0.6$. Third, to illustrate the species-diagnosticity of the mitochondrial 16S, we conducted a similar analysis on 66 identified 16S haplotypes (~450 bp aligned).

All three analyses were run for 50 million iterations, sampling every 5,000, and checked for stationarity and effective sample sizes of parameters with Tracer v. 1.5. Trees were visualized using DensiTree 2.0 (Bouckaert and Heled, 2014), and summarized into maximum-clade credibility trees with the module TreeAnnotator, discarding the first 20% of trees as burnin.

Finally, we further detailed haplotype relationships within three rich and widespread mitochondrial CR clades from the eastern Mediterranean and Central Asia, by haplotype networks (R package *pegas*, Paradis, 2010).

2.1.6. Genome size

The amount of DNA per nucleus, i.e. genome size, provides an *ad hoc* index to distinguish between diploid and polyploid individuals, but also between closely-related diploid species (e.g. Litvinchuk et al., 2011, Faizulin et al., 2018). We compiled published data on 1,167 individuals and examined 1,309 new ones, for a total of 2,476 individuals from 472 known localities (Table S3). Specimens were collected over the 1985–2018 period and deposited at the herpetological collections of the Zoological Institute, Russian Academy of Science, St. Petersburg (ZISP, St. Petersburg, Russia) and the Museum of Nature V. N. Karazin Kharkiv National University (KUMN, Kharkiv, Ukraine).

Genome size was measured by DNA flow cytometry with a microscope-based flow fluorimeter using a mercury arc lamp as a light source (Institute of Cytology, Russian Academy of Sciences, St. Petersburg, Russia), with optimized conditions of fluorescence excitation and registration. Details of the techniques can be found in Vinogradov et al., 1990, Rosanov and Vinogradov, 1998, Borkin et al., 2001a. Briefly, red blood cells were taken from the heart or from the femoral vein, and mixed with blood cells of *Rana temporaria* (the reference standard, 10.32 pg; Borkin et al., 2001a). Cell samples were suspended in phosphate buffer saline, supplemented with 0.7 mM EDTA (pH 7.5), with a total cell concentration of approximately 106 cells/ml. Cells were lysed by addition of Triton X-100 (Ferak, Berlin; 0.1%), and stained with a mixture of

olivomycin (OM, Moscow Medicine Plant; 40 µg/ml), ethidium bromide (EB, Calbiochem; 20 µg/ml) and $MgCl_2$ (15 mM). Stained cell samples were measured 24 h later at +4 °C. To account for the potential influence of AT/GC structure (see Vinogradov and Borkin, 1993), several samples from each species were also stained with ethidium bromide only, and measured 4–6 h later. Each sample was run four times, combining more than 10,000 cells measured, and the estimated genome size was obtained by fitting a Gaussian curve to the peak distribution.

We made comparisons between taxa by Tukey tests (accounting for multiple comparisons). For the parapatric *B. sitibundus* and *B. viridis*, we did not include potential hybrid populations in the species comparisons (Faizulin et al., 2018), but applied the threshold of Faizulin et al. (2018) for species delimitation, i.e. <9.62 pg for "pure" *B. sitibundus* and >9.76 pg for "pure" *B. viridis*.

2.2. Phenotypic analyses

2.2.1. Bioacoustics

We compared advertisement calls between most species of the *Bufotes* radiation, combining our own field recordings with those available from online sources (Table S4). Green toad calls are perceived as monotonous trills made of series of pulses, and vary depending on the motivation and environmental context (Köhler et al., 2017). Because of the heterogeneous qualities of recordings, we lacked information on temperature, a factor affecting temporal call features (Castellano et al., 1999, Stöck et al., 2001b), as well as body size, which affects spectral call features (Castellano et al., 1999). To accommodate these uncertainties, we thus limited our analyses to single notes and two variables that we could reliably measure and compare: the fundamental frequency of the call (F_f, in kHz) and the pulse rate (PR), i.e. the number of trills per second (in s^{-1}).

A total of 84 recordings from different individuals were processed as follows (Table S4). We first used the software Audacity (available at https://www.audacityteam.org/) to explore and isolate individual calls, ideally free of background noise, e.g. from overlaying toads and wind. These notes were subsequently analyzed with the *R* package *seewave* (Sueur et al., 2008). We filtered out background noise below 0.8 kHz and above 2.5 kHz (outside of the *Bufotes* spectrum; function *ffilter*), checked the resulting profile (function *spectro*), computed F_f (function *fpeaks*) and visually inferred PR from the oscillogram, framed to one second of call (function *cutw*). Finally, we supplemented this dataset by published F_f and PR values from 29 additional Central Asian toads, for a total of 113 individuals included in the comparisons (Table S4).

2.2.2. Toxin composition

Toxin samples were obtained from the parotoids of 71 individuals, representing eight *Bufotes* species (of all three ploidy levels) as well as four closely-related bufonids (*Duttaphrynus melanostictus*, *D. stomaticus*, *D. himalayanus,* and *Sclerophrys mauritanicus*) (Table S5). Their composition was analyzed by gas chromatography and mass spectrometry, which have proven powerful in amphibians (reviewed in Daly et al., 2005). Dried skins were flash frozen with liquid nitrogen, grinded with a mortar and subsequently extracted in HPLC-grade chloroform in a total volume of 1 ml. Samples were analyzed on a gas chromatograph (Thermo Fisher Scientific Trace 1300 series) coupled with a mass spectrometer (Thermo Fisher Scientific ISQ series MS) (GCMS). We used a volume of 1 µL and splitless injection with an inlet temperature of 320 °C. The initial temperature of 40 °C was held for 1′, then increased to 200 °C at a rate of

20 °C/min and then up to 340 °C at a rate of 8 °C/min, finally held for 4 min. Helium was used as a carrier gas at a constant flow rate of 0.9 ml/min. The electron ionization voltage was autotuned to enhance the acquisition performance according to the molecular weight of the compounds (up to 600 g/mol, while known bufotoxins range ~150–550 g/mol, Daly et al., 2005). Three pure standards were used in the analysis: bufotenin (204.3 g/mol), gamabufotalin (402.5 g/mol) and arenobufagin (416.5 g/mol), all within the detection limits of the GCMS. The MS transfer line temperature was set to 320 °C and the ion source temperature to 300 °C. The column used was a Restek RXi-5sil MS 20 m with an internal diameter of 0.18 mm and a film thickness of 0.18 μm. Peaks in the total ion chromatogram were aligned and integrated using a custom R script (available on request). We used Aitchison (centered log-ratio) transformed absolute abundances of the fourteen major toxins (Aitchison, 1982). We then performed a PCA (R package *FactoMineR*, Lê et al., 2008) and a social network analysis with the adjacency matrix of the toxin chemical data (R package *igraph*, Csardi and Nepusz, 2006).

2.2.3. Morphometrics

Body size (snout-vent length, SVL) and sixteen morphometric variables were measured in 140 museum specimens of known origins, curated at the Museum National d'Histoire Naturelle (MNHN, Paris), the Zoologische Staatssammlung München (ZSM), the Museum d'Histoire Naturelle de Genève (MHNG), the Zoological Institute of St. Petersburg (ZISP), the Museum für Tierkunde Dresden (MTD), and the Uppsala Universitets Zoologiska Museum (ZIUU), representing all *Bufotes* species, and including their type series for several (Table S6a). Variables were corrected for body size (SVL-divided ratio) and the dataset was analyzed by means of PCA, MANOVA, and Tukey tests in *R*, accounting for the sex of individuals.

Furthermore, we gathered average body sizes (SVL) from an additional 195 published sample sets, representing more than 6000 toads in total (Table S6b), for range-wide comparisons between taxa.

2.3. Species distribution modelling

We modelled distributions under past and present environmental conditions for the fifteen identified *Bufotes* species (see Section 3) with MaxEnt (ver. 3.4.1; Phillips et al., 2006). To infer the ecological niches, we considered 6240 localities based on published and our own records (listed in Table S7), filtered to avoid spatial autocorrelation and duplication (ENMTools 1.3, Warren et al., 2010).

Altitude and nineteen bioclimatic layers were separately extracted from the WorldClim 1.4 database (http://www.worldclim.org) for present-day conditions (~1950–2000) and during the last glacial maximum (LGM, ~22,000 years ago). For contemporary predictions, we considered three additional layers: the aridity index (http://www.cgiar-csi.org/data/global-aridity-and-pet-database), spatial homogeneity of global habitat (http://www.earthenv.org/texture.html) and global percent of tree coverage (https://github.com/globalmaps/gm_ve_v1). Four additional topographic layers were computed with QGIS (aspect, exposition, slope, and terrain roughness index). We applied two general atmospheric circulation models to generate LGM climate scenarios: the Community Climate System Model (CCSM; http://www2.cesm.ucar.edu/) and the Model for Interdisciplinary Research on Climate (MIROC; Watanabe et al., 2011), framed with a mask that extended from 15°N to 63°N and 20°W to 97°E. Spatial resolution was 30 arc-seconds (~1 km) for contemporary layers, on which 6059 filtered localities were considered in the models. The layers used for LGM projections were of 2.5 arc-minutes resolution (~5 km).

To eliminate predictor collinearity, we first calculated Pearsons's correlation coefficients for all pairs of bioclimatic variables using ENMTools, excluding the variable from a correlated pair ($|r| > 0.75$) that we considered to be the less biologically important, based on known preferences of *Bufotes* toads. The resulting dataset contained nine bioclimatic variables: Bio2 (mean diurnal range; °C × 10), Bio7 (temperature annual range; °C × 10), Bio8 (mean temperature of wettest quarter; °C × 10), Bio9 (mean temperature of driest quarter; °C × 10), Bio14 (precipitation of driest month; mm), Bio15 (precipitation seasonality; CV), Bio16 (precipitation of wettest quarter, mm), Bio18 (precipitation of warmest quarter, mm), and Bio19 (precipitation of coldest quarter, mm), bringing to 17 the total variables considered in the models.

Model performance was measured using the Area Under the Curve (AUC) derived from the Receiver Operating Characteristic (ROC) plots. We used default settings in MaxEnt (30 replicates), i.e. a regularization multiplier of 1, all feature classes, 500 iterations maximum and 10,000 background points maximum (Phillips and Dudík, 2008). Finally, we applied a jackknife analysis for estimating the relative contributions of variables to the MaxEnt model.

2.4. Taxonomic analyses

2.4.1. Genetic analysis of the type series of B. turanensis *Hemmer, Schmidtler, Böhme, 1978*

Two diploid green toad lineages were distinguished in Central Asia from previous work: one is restricted along the Amu-Darya River, assigned to *B. shaartusiensis* (Pisanets et al., 1996) since Litvinchuk et al. (2011); the other is widespread across Iran, Turkmenistan, Uzbekistan, Tajikistan and Kazakhstan, assigned to *B. turanensis* since Stöck et al. (2006). Yet, both type localities are situated close-by and potentially inhabited by either taxa.

To clarify this situation, we genotyped the type series of *B. turanensis* (holotype MTD 11195 and nine paratypes, all from the type locality: Dushanbe, Tajikistan; Table S1) at five microsatellite loci (C201, B118, C105, D115, D5), to be compared with genotypes published by Betto-Colliard et al. (2015) from Bishkek, Kyrgyzstan (assigned to *B. turanensis*, $n = 6$) and Shaartuz, Tajikistan (the type locality of *B. shaartusiensis*; $n = 4$). DNA was obtained from skeletal muscle tissues and extracted with the DNeasy kit (Qiagen). To make sure of allele correspondence with the data of Betto-Colliard et al. (2015), we applied their PCR protocol and primers, used the same genotyping machine (an ABI3130 genetic analyzer at the University of Lausanne) and called alleles with the original bin panels designed by CB-C in Genemapper 4.0 (ABI). One marker (C105) was monomorphic in all samples and was subsequently discarded. The remaining four were analyzed by a PCA on allele frequency (R package *adegenet*) and a STRUCTURE analysis for $K = 1–4$, including 10 replicate runs per K, each of 100,000 iterations after a burnin of 10,000, using the admixture model with independent allele frequency.

Mitochondrial sequences from the type series were also generated. We initially sequenced 16S in all the analyzed types (methods in Section 2.1.3), but only ~200 bp overlapped to our haplotype catalog. Then, to confirm the mitochondrial identity of the holotype MTD 11195, we sequenced its full mitogenome. Shotgun library preparation was performed using NEBNext® Ultra™ DNA Library Prep Kit for Illumina® with individual indexing. Two lanes of paired-end 100 bp sequencing data were obtained from the Illumina HiSeq 2500 System at the LGTF (University of Lausanne, Switzerland). We used NOVOPlasty 3.1 by Dierckxsens et al. (2016) for the initial assembly and the two resulting contigs were mapped to the complete mitochondrial sequence of the related species *Strauchbufo raddei* (Genbank NC_028424).

Ultimately, the raw reads were re-mapped on the resulting consensus in Geneious 8.1.9, and the circularized mitochondrial chromosome sequence was annotated by MITOS 2 (Bernt et al., 2013). We then harvested full CR and 16S sequences to be matched against our haplotype catalogs for these markers (see Section 2.1.3).

2.4.2. Distributions and available taxonomic names

Combined with our new data, we reviewed published literature on *Bufotes* distribution to refine range limits with ArcMap 10.5 (ArcGIS). A total of 60 publications were considered (Table S8). In addition, we explored the taxonomic literature on *Bufotes* as listed by Frost (2019), to identify available nomina, junior synonyms, and map the type localities of recognized and debated taxa.

2.4.3. Descriptions of new taxa

In order to describe two new species (see 4.3.4 , 4.3.5), type specimens were collected from genetically identified populations and registered into scientific collections (MHNG, KUMN, ZISP). All but one individual (mummified) were fixed in 70% ethanol, and later examined, measured, and photographed post-mortem.

For each species, high-quality spectrograms and oscillograms of advertisement calls were produced using *seewave* (see Section 2.2.1). We further prepared karyotypes following the methodology of Litvinchuk et al. (2017). Briefly, this consists of injection of colchicine (0.4%) into the specimen and treatment of intestine cells by a hypotonic KCl solution (0.07 M) and fixation by acetic acid – methanol (1:3). For the production of metaphase plates, the treated tissue fragments were kept in 60% acetic acid water solution, and the cell suspension was dropped on glass slides heated up to 60 °C. Conventional chromosome staining (Giemsa and C-banding) and labeling of the Nucleolus Organizer Regions (NORs) with $AgNO_3$ were further performed following Schmid et al. (2010).

To highlight cranial differences between the newly-described taxon from Central Asia (see Section 4.3.5) and its sympatric congener *B. turanensis*, we conducted morphological reconstruction of the cranium and mandible from four museum specimens, including the holotypes. Heads were X-rayed in 3D with a high-resolution micro-CT scanner (Bruker SkyScan 1173) at ZFMK, Germany. CT-scanning was performed in 180° (rotation step of 0.4°) under tube voltage of 70 kV and a current of 114 μA (0.5 mm Al filter), with image resolution of 19.65 μm, and exposure time of 600 ms during 42–44′. The CT data were reconstructed using N-Recon software v1.7.1.6 (Bruker MicroCT), and 3D rendering was computed with CTVox (Bruker MicroCT).

3. Results

3.1. Genetic analyses

3.1.1. Genomic inferences

Based on 615 SNPs sequenced across the entire radiation ($n = 136$ individuals), STRUCTURE recovered eight genetic clusters ($K = 8$) corresponding to several diploid taxa or pairs of taxa (Fig. 1): (i) *B. boulengeri* (yellow circles) in North Africa (*B. b. boulengeri*) and Sicily (*B. b. siculus*); (ii) *B. balearicus* (dark green circles) in the Apennine Peninsula; (iii) *B. viridis* (light

green circles) occupying most of Europe, but also present in northwestern Anatolia (vr13) and Siberia (vr9); (iv) the Middle-Eastern lineage (blue circles), which corresponds to *B. sitibundus* (see Section 4.3.1); (v) a new taxon endemic to Cyprus (white circles), described below as *B. cypriensis* sp. nov. (see Section 4.3.4); (vi) the Amudaryan species (purple circles), which corresponds to *B. turanensis* (see Section 4.3.3); (vii) a Central Asian lineage (brown circles), described below as *B. perrini* sp. nov. (see Section 4.3.5); (viii) the sister species *B. surdus* and *B. latastii* (grey circles), merged into a single cluster (but see below). The PCA discriminated between most taxa, including *B. b. boulengeri vs B. b. siculus*, and *B. surdus vs B. latastii* (Fig. 2).
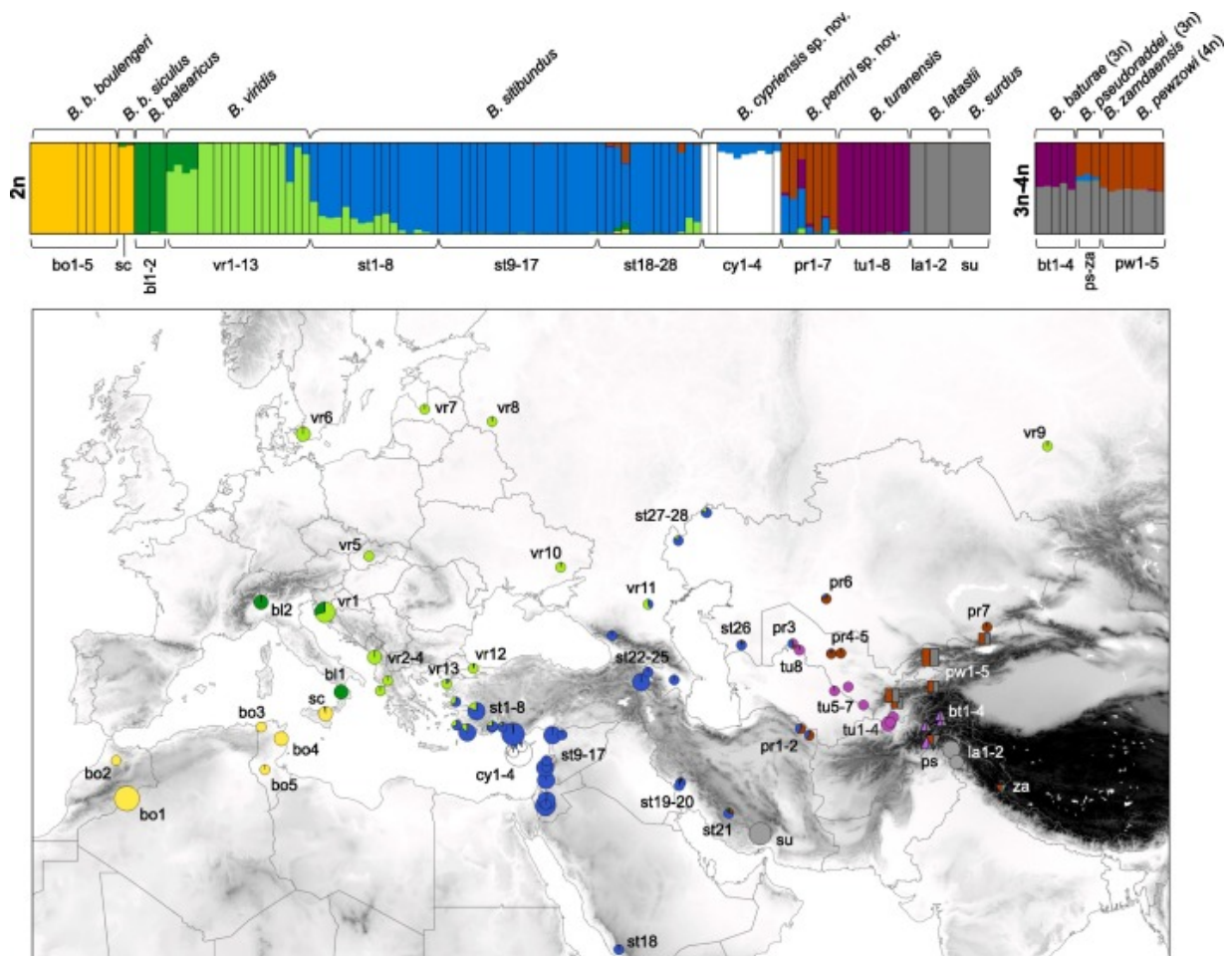
Fig. 1. Individual assignments (barplots) and geographic distribution (map) of STRUCTURE nuclear clusters ($K = 8$) in 136 toads from 82 populations, based on 615 nuclear SNPs sequenced across the *Bufotes* genus; pie size is proportional to sample size. Symbols indicate ploidy: circles, triangles, squares represent diploids (2n), triploids (3n) and tetraploids (4n), respectively.
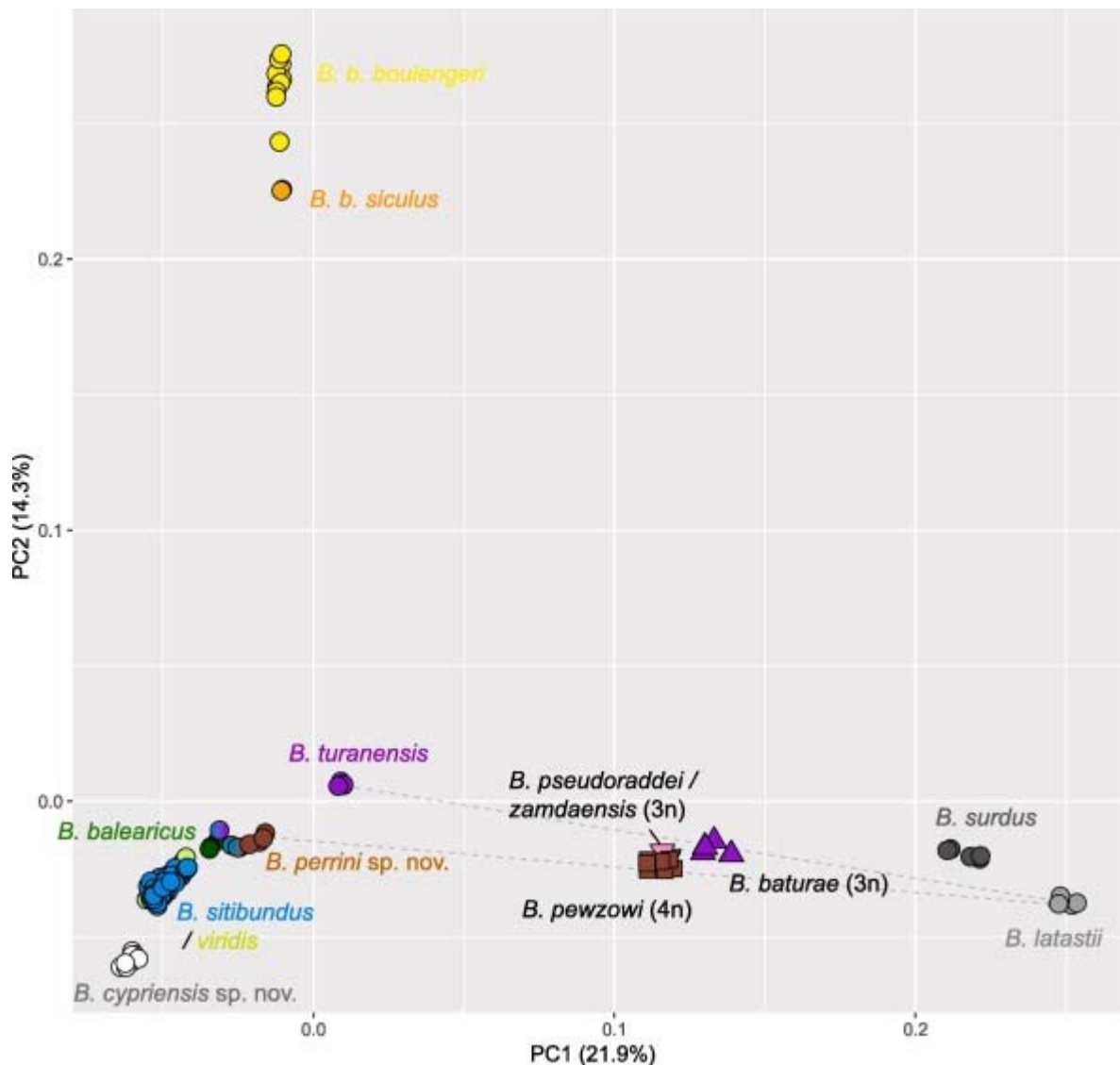
Fig. 2. Principal Component Analysis (PCA) based on 615 nuclear SNPs sequenced across the *Bufotes* genus. Points represent individuals, colored by taxa and shaped by ploidy (circles: 2n, triangles: 3n, squares: 4n). The dash lines illustrate how hybrid species clustered intermediately from their respective parents.

Genomic analyses on subsets of taxa fine-tuned the resolution. In the E-Mediterranean (1432 SNPs), we mapped a transition zone between *B. viridis* and *B. sitibundus* spanning across W-Anatolia, and detected *B. sitibundus*-like alleles on Cyprus (Fig. 3A). The analysis also contrasts *B. sitibundus* populations from the southern Levant/Saudi Arabia (st11-18) *vs* the rest of the range, with widespread admixture. In Central Asia (433 SNPs), *B. latastii* and *B. surdus* are distinguished. Many populations are admixed between *B. sitibundus* and *B. perrini* sp. nov., but gene flow was absent with *B. turanensis*, except at one site (pr3, a triple hybrid individual; Fig. 4A). Note that the likelihoods of STRUCTURE runs did not increase above the *K* values reported (Fig. S2), for which no additional structure arose.
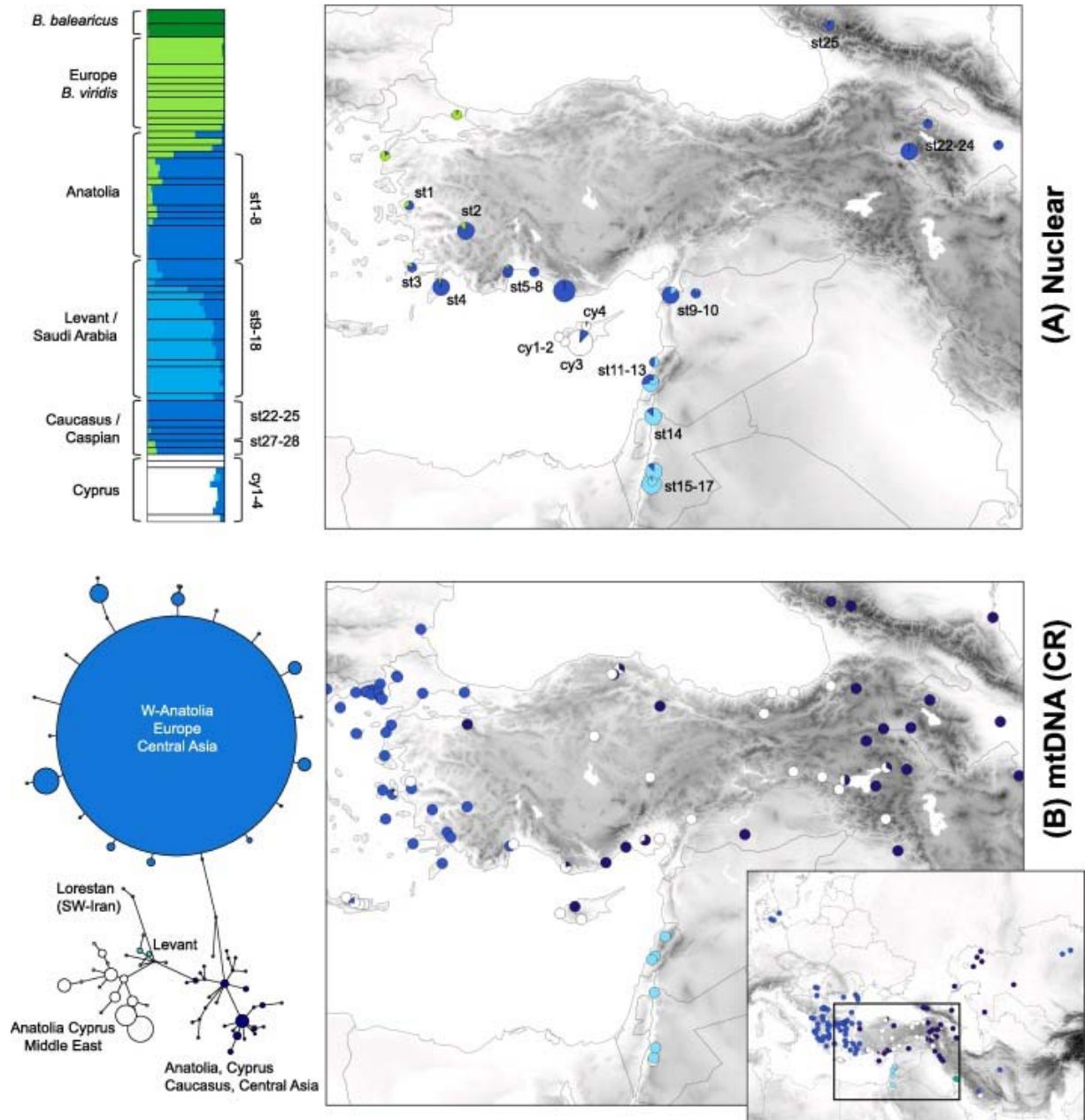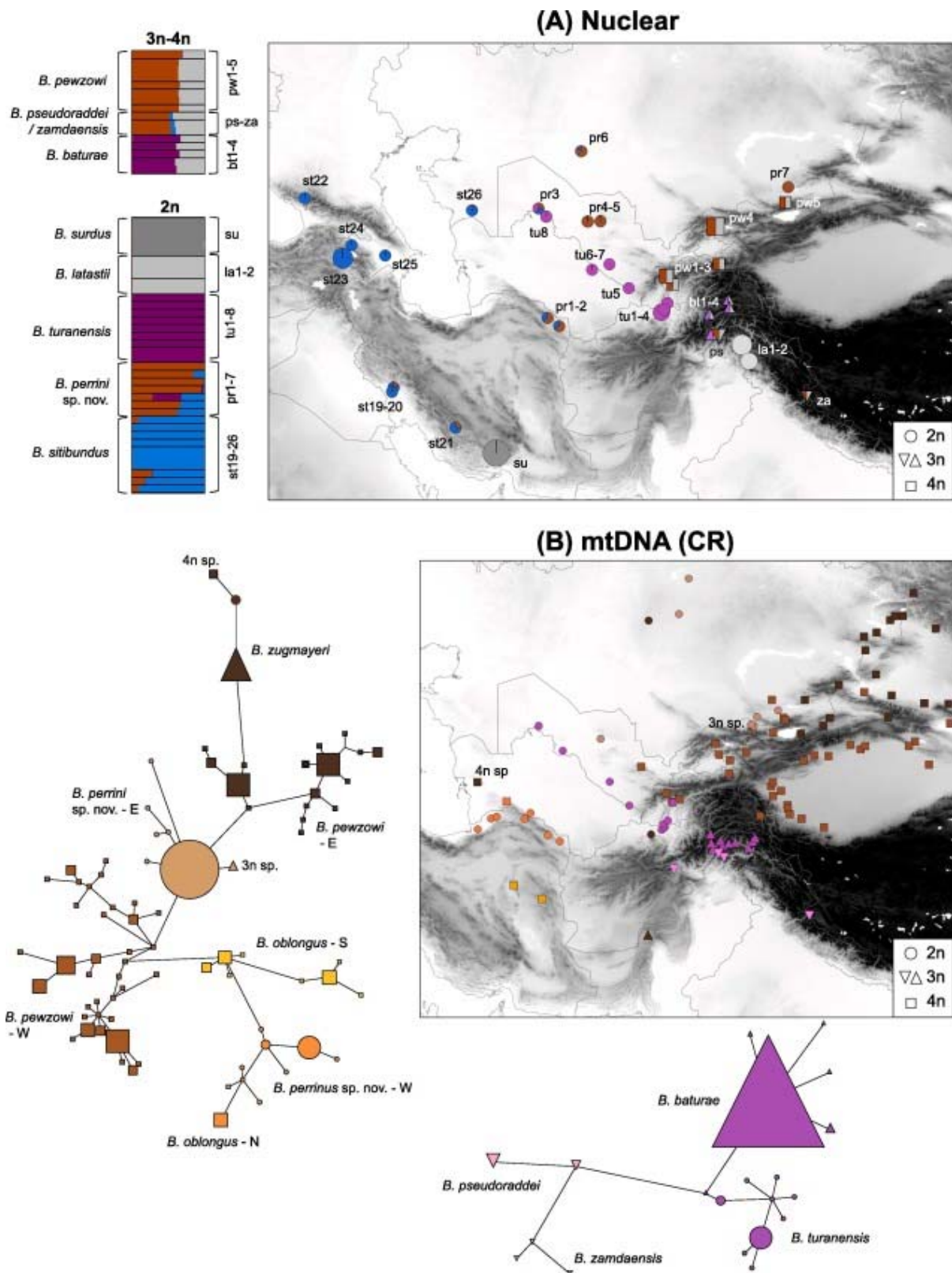
Fig. 3. Phylogeography of Eastern-Mediterranean green toads. (A) Individual assignments (barplots) and distribution (map) of STRUCTURE nuclear clusters (*K* = 5) in 76 individuals from 42 populations, based on 1432 SNPs; pie chart size is proportional to sample size. (B) Haplotype network of the control region (CR) mitochondrial haplotypes of *B. sitibundus*, colored by haplogroups and mapped across Eurasia. (For interpretation of the references to color in this figure legend, the reader is referred to the web version of this article)

Fig. 4. Phylogeography of Central Asian green toad populations. (A) Individual assignments (barplot) and distribution (map) of STRUCTURE nuclear clusters ($K = 5$) in 52 individuals from 37 populations, based on 433 SNPs; pie chart size is proportional to sample size. (B) Haplotype networks of the control region (CR) mitochondrial haplotypes from the *B. perrini* sp. nov. and *B. turanensis* clades and mapped across Central Asia; symbols indicate the ploidy of the toads carrying each haplotype. (For interpretation of the references to color in this figure legend, the reader is referred to the web version of this article)

From these analyses, we could infer the nuclear background of four hybrid species (Fig. 1, Fig. 2, Fig. 3, Fig. 4): (i) the triploid *B. baturae* as *B. latastii* × *B. turanensis*; (ii) the triploids *B. pseudoraddei* and *B. zamdaensis* as *B. latastii* × *B. perrini* sp. nov. (introgressed by *B. sitibundus*); and (iii) the tetraploid *B. pewzowi* as *B. latastii* × *B. perrini* sp. nov.
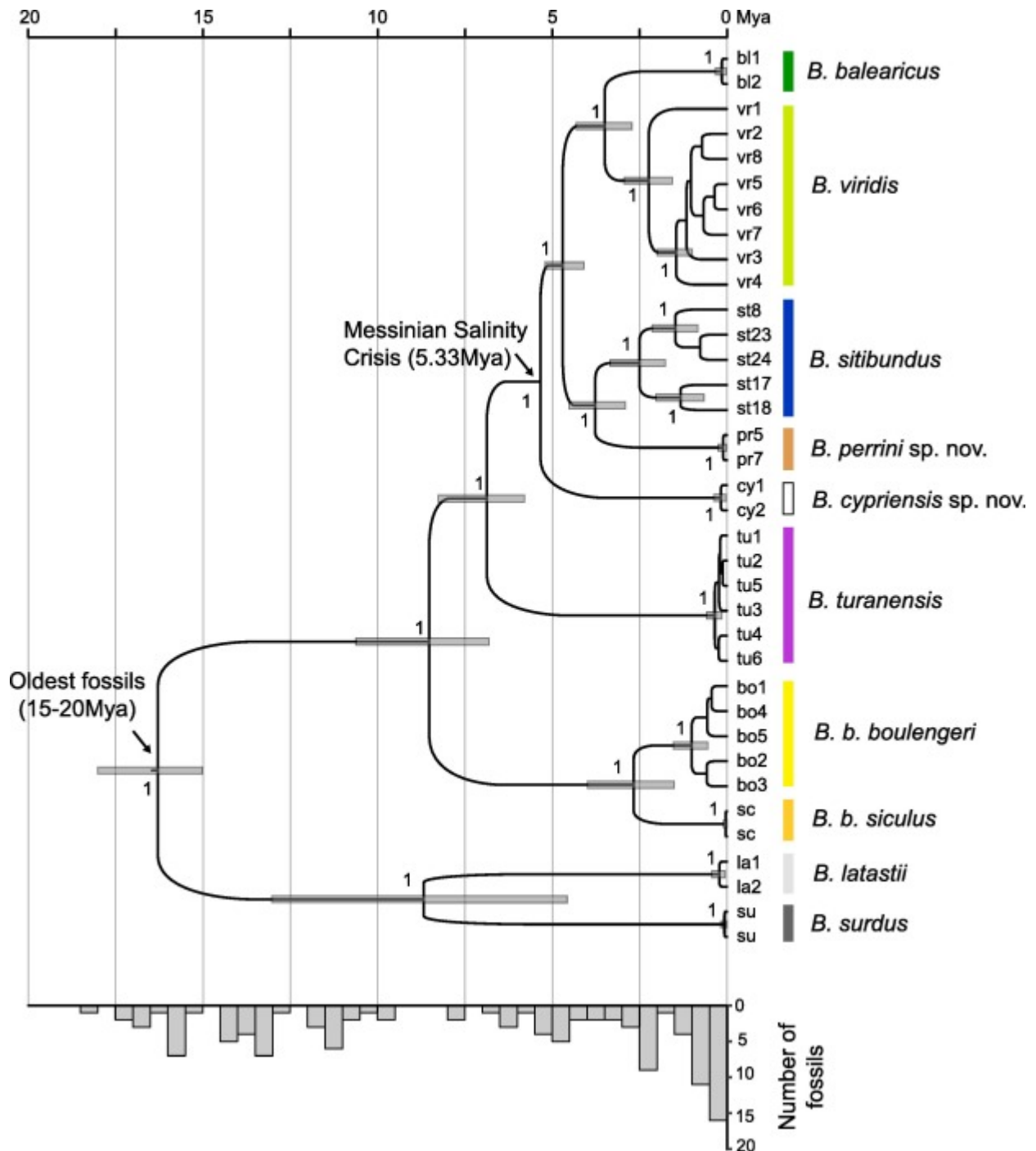

Fig. 5. Time-calibrated nuclear phylogeny of the *Bufotes* radiation based on ~45 bp of RAD tags sequenced in 36 diploid specimens (labels indicate geographic origin as shown in Fig. 1, Fig. 2, Fig. 3, Fig. 4; see Table S1 for details). A DensiTree display is available as Fig. S3a. The bottom charts illustrates the respective amount of fossils identified as *Bufotes* through time (mapped in Fig. S1).

We provide a fully-resolved nuclear phylogeny for all diploid green toads (Fig. 5, Fig. S3a), except *B. luristanicus* which was not sequenced. According to fossil evidence, the *B. latastii* and *B. viridis* groups diverged at least 15 Mya (Fig. 5), and the latter progressively diversified during the upper Miocene (8.5 Mya for *B. boulengeri*; 6.9 Mya for *B. turanensis*), at the Messinian Salinity Crisis (5.3 Mya for *B. cypriensis* sp. nov.; used as a second calibration point in final analyses), and during the Pliocene (4.7–3.5 Mya for *B. viridis*, *B. balearicus*, *B. sitibundus* and *B. perrini* sp. nov.). In the *B. latastii* group, the branch leading to *B. surdus* is as old as 8.6 Mya. The tree also confirmed the early split of *B. viridis* from the NE-Adriatic (vr1) and *B. sitibundus* from the Levant/Saudi Arabia (st17-18).

3.1.2. Mitochondrial inferences

The mitochondrial control region (CR) recovered 14 major clades (Fig. 6, Fig. S3b), with a robust internal topology congruent with the nuclear phylogeny (Fig. 5), but poorly resolved relationships among recent nodes. Combined with 16S barcoding data (see Fig. S3c), these clades could be accurately mapped in 636 localities throughout Eurasia (Fig. 6).

Several CR clades featured high intraspecific variation. First, *B. sitibundus* is composed of four distinct haplogroups, broadly distributed in western (W-Anatolia and Europe; blue), central (Anatolia and Cyprus; white), eastern (the Caucasus and Central Asia; dark blue) and southern ranges (Levant and Saudi Arabia; cyan), with wide overlaps (Fig. 3B). In the W-Anatolian/European haplogroup, a single haplotype was fixed across most populations (SIT12). Second, Central Asian lineages diversified in respect to geography and divergence among diploid and polyploid species (Fig. 4B). We recovered two main CR clades associated with the diploid *B. perrini* sp. nov.: in the west (Iran, SW-Turkmenistan) and in the east (China, Kazakhstan, Uzbekistan, Tajikistan, Afghanistan and Kyrgyzstan). The western clade diversified in N-Iran/SW Turkmenistan (diploid *B. perrini* sp. nov. – W, tetraploid *B. oblongus* – N; light orange) and Central Iran (tetraploid *B. oblongus* – S; gold). The eastern clade is more complex, with separate haplogroups found in diploid *B. perrini* sp. nov. (E, light brown) and tetraploid *B. pewzowi* from southwestern (W, brown) and northeastern ranges (E, dark brown). The latter include haplotypes fixed in the triploid *B. zugmayeri*, in a tetraploid form isolated in the Bolshoi Balkhan ridge in western Turkmenistan (4n sp.), and in presumed diploids from Kazakhstan and northern Afghanistan. Third, the mitochondrial diversity associated with the diploid *B. turanensis* can be summarized in two haplogroups: a northern one in the diploid *B. turanensis* and the triploid *B. baturae* (purple), and a southern one restricted to the triploids *B. pseudoraddei/zamdaensis* (pink).

By comparing the nuclear and mitochondrial perspectives, we outline several range-wide cases of cyto-nuclear discordance: (i) the Cyprian endemic *B. cypriensis* sp. nov. possesses *B. sitibundus* mtDNA of Anatolian origin, with haplotypes identical or weakly-differentiated to those from the continent (Fig. 3, Fig. S3b and c); (ii) many European populations have fixed *B. sitibundus* mtDNA from the W-Anatolian haplogroup, despite an exclusive *B. viridis* nuclear ancestry (Fig. 1, Fig. 2); (iii) the mitochondrial divergence of western *B. perrini* sp. nov. populations is not mirrored by the RAD data, which instead suggest a *B. perrini* sp. nov./*B. sitibundus* hybrid ancestry; (iv) the mtDNA of *B. luristanicus* branches within the *B. viridis/balearicus/perrini* sp. nov./*sitibundus* clade, while this species is related to *B. surdus*; (v) the triploids *B. pseudoraddei/zamdaensis* bear mtDNA of *B. turanensis* origin, despite a *B. perrini* sp. nov./*B. latastii* nuclear background.
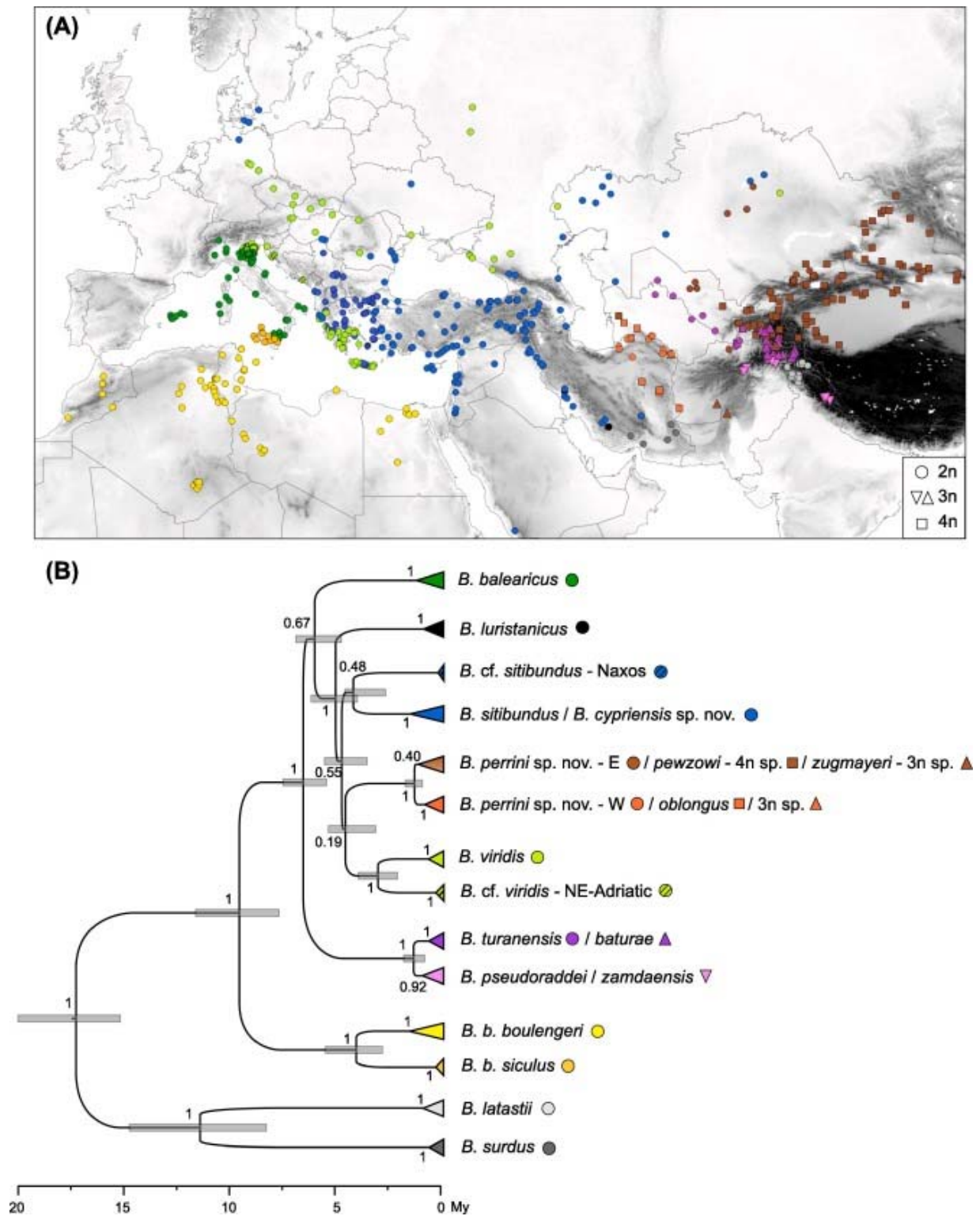
Fig. 6. Distribution and phylogenetic relationships among the main *Bufotes* mitochondrial lineages. (A) Geographic locations of 636 localities barcoded with either the control region (CR) or 16S gene, combining own and literature data. (B) Time-calibrated phylogenetic tree of the CR (~850 bp), trimmed to the main clades for visibility. Full haplotype trees are available in Fig. S3b.

3.1.3. Genome size inferences

Genome size offered complementary insights on species ranges, differentiation and hybridization (Fig. 7). Genomes were 20% larger in the *B. latastii* group (12.1 pg on average) than in the *B. viridis* group (10.1 pg on average), and we found significant variation among most species, including close relatives (Tables S9–S10). First, we could map the parapatric ranges of *B. sitibundus* and *B. viridis* in Eastern Europe (from the Ural to the Caucasus) and northwestern Anatolia (Fig. 7), in congruence with the RAD data (see Section 3.1.1). Second, we fine-tuned the distributions of *B. pewzowi* and *B. baturae* in the Pamirs, combining genome size and mtDNA barcoding (Fig. S4). Both species have mosaic distributions and were presumably found in syntopy at only two sites in SW-Tajikistan (Shakhdara River, Sangmar-Mar), but a few individuals identified as triploid *B. baturae* possessed *B. pewzowi* mtDNA, and vice versa (Fig. S4). Third, toad genome size was significantly lower in western than eastern populations of *B. perrini* sp. nov., consistent with introgression by the small genome of *B. sitibundus* in the former. Fourth, genomes did not significantly differ in size between the presumably sister species *B. surdus* and *B. luristanicus*.

Finally, genome size supported distinct origins between the triploids *B. pseudoraddei* (*zamdaensis*) and *B. baturae*: their shifted estimates mirrored the variation between their respective maternal ancestors (Fig. 7). East-west differences in *B. perrini* sp. nov. is also reflected in their associated tetraploids: the western *B. oblongus* has a smaller genome than the eastern *B. pewzowi*, a trend that holds true for the presumably related triploids found in Iran and Kyrgyzstan/Kazakhstan, respectively (3n sp., Fig. 7, Tables S9–S10).

3.2. Phenotypic analyses

3.2.1. Bioacoustics

Breeding calls can be classified in three broadly overlapping categories (Fig. 8, Table S9): (i) slow (PR ≈ 7.6 trills s^{-1}) and high-pitched (F$_f \approx 1.73$ kHz) in the *B. latastii* group; (ii) fast (PR ≈ 23.6 trills s^{-1}) and medium-pitched (F$_f \approx 1.34$ kHz) in the *B. viridis* group, except for (iii) the Amudaryan endemic *B. turanensis*, which featured unique, very fast (PR ≈ 47.8 trills s^{-1}) and lower-pitched (F$_f \approx 1.12$ kHz) notes.

The hybrid taxa exhibited broadly intermediate call properties between the *B. viridis* group (*B. turanensis* excepted) and *B. latastii* group (PR ≈ 16.7 trills s^{-1}; F$_f \approx 1.46$ kHz) (Fig. 8). Accordingly, a MANOVA combining F$_f$ and PR highlighted a significant group effect ($P < 0.001$). Pairwise comparisons between each species are detailed in Table S11.
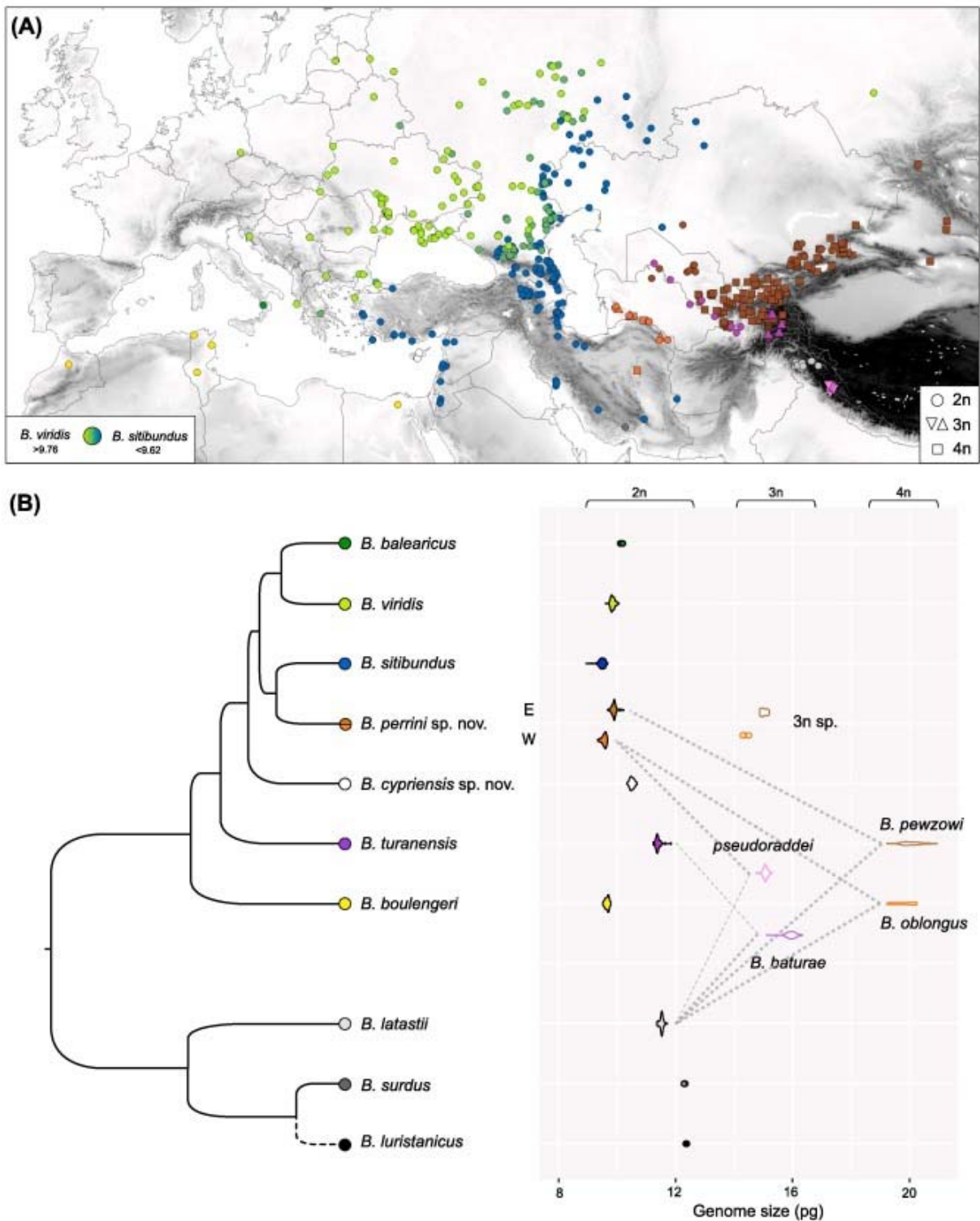
Fig. 7. Variation in genome size (GS) across the *Bufotes* radiation. (A) Localities barcoded with GS, based on own and known records; the threshold by Faizulin et al. (2018) was used to distinguish *B. sitibundus* and *B. viridis*. (B) Violin plots for each species arranged along the phylogeny (circles when *n* < 3); western and eastern populations of *B. perrini* sp. nov. are displayed separately; dash lines illustrate the origin of polyploids (thin: contribution of one genome set; thick: contribution of two genome sets); the phylogenetic position of *B. luristanicus* is taken from Betto-Colliard et al. (2018).
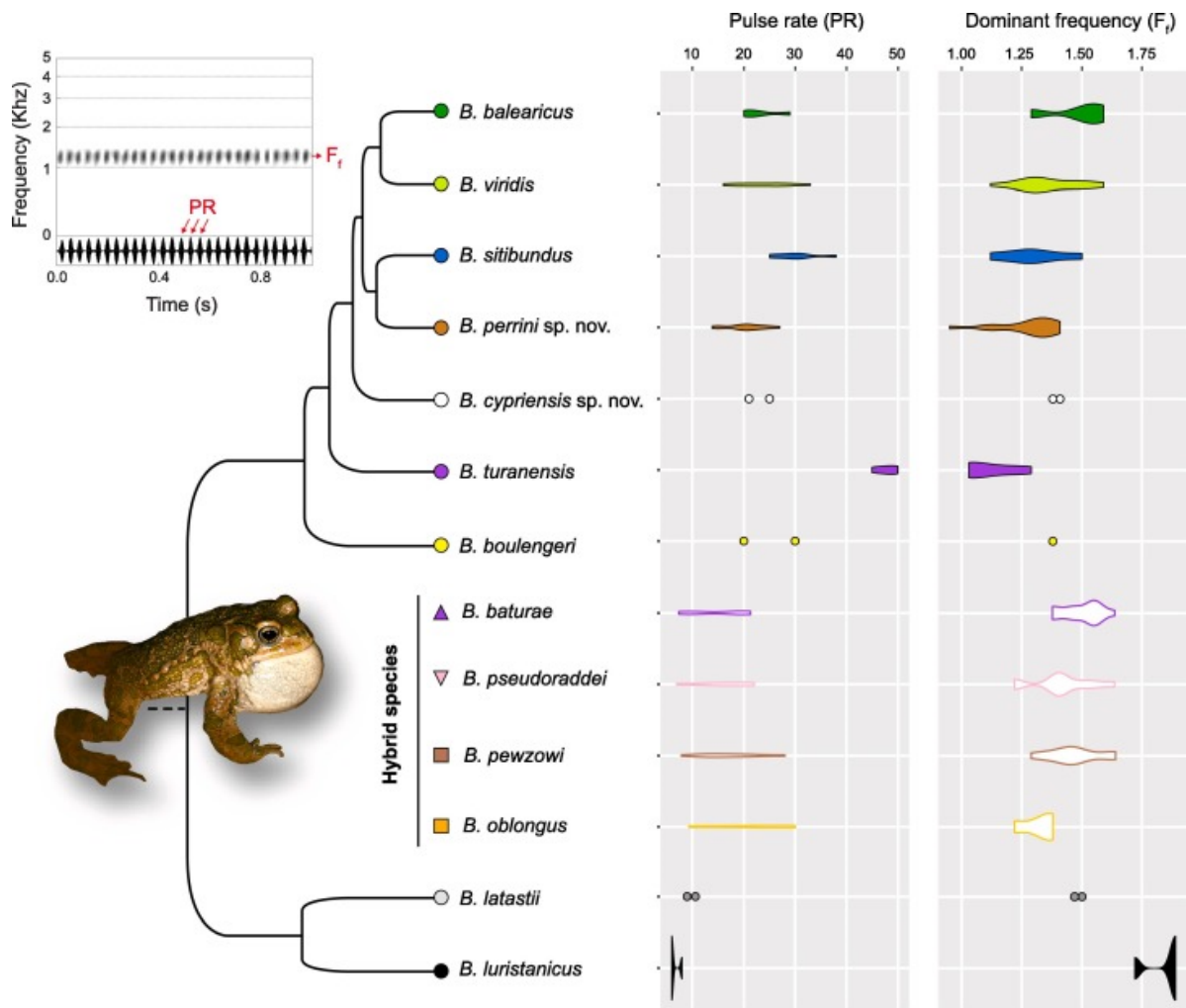
Fig. 8. Variation in the two main parameters of *Bufotes* breeding calls, arranged along the species tree (hybrid taxa in the middle); violin plots are used for $n > 3$. The upper-left diagram illustrates the pulse rate (PR, in s^{-1}) and the fundamental frequency (F_f, in kHz) of a call (taken from *B. viridis*). Photo credit: Dennis Hägg.

3.2.2. Toxin composition

Four out of the fourteen chemicals isolated were identified, namely as Bufotenin, Arenobufagine, Gelebrigenin and Gamabufotalin. Considering only *Bufotes*, the latter three contributed about 75% of the variance explained by the first two components of the PCA (Fig. 9A), which separated the mountainous *B. latastii*, *B. baturae* and *B. pseudoraddei*, from the cosmopolitan *B. viridis* group (*B. viridis*, *B. sitibundus*, *B. perrini* sp. nov. and *B. turanensis*) and *B. pewzowi*, the latter showing strong variation between individuals. The network analysis confirmed these results and further contrasted *Bufotes* from the other bufonids analyzed (*Sclerophrys* and *Duttaphrynus*) (Fig. 9B).
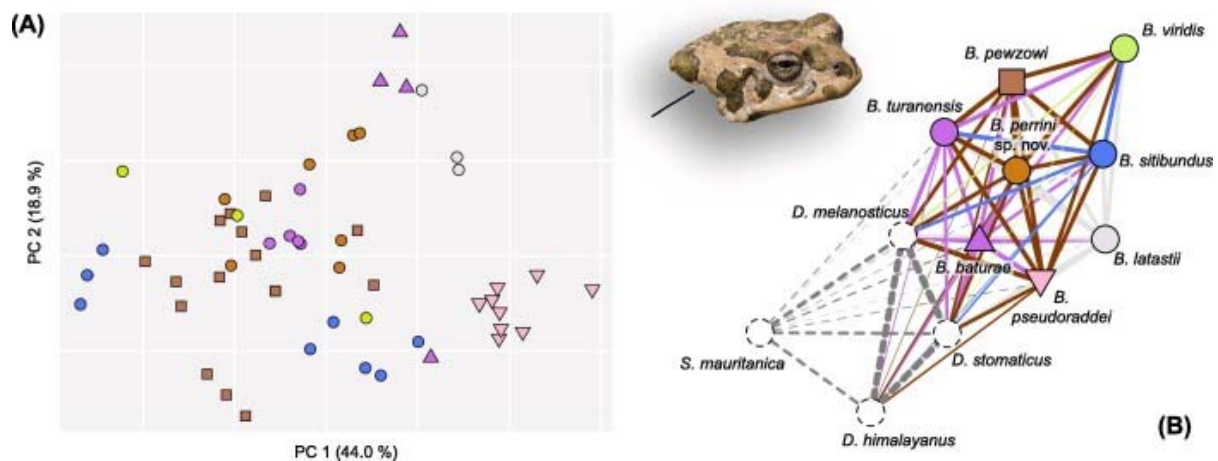
Fig. 9. Toxin similarities between green toad species, based on 14 isolated chemical compounds. (A) PCA analysis on *Bufotes* individuals: each point represents an individual, coded by species (color) and ploidy (shape; 2n: circles, 3n: triangles, 4n: rectangles). (B) Social network diagram showing the relationships among *Bufotes* and four related bufonids from the *Sclerophrys* and *Duttaphrynus* genera. Photo credit: DJ (*B. pewzowi* from Kazakhstan). (For interpretation of the references to color in this figure legend, the reader is referred to the web version of this article.)

3.2.3. Morphometrics

A MANOVA on 17 morphometric variables highlighted the global effects of species and sex ($P < 0.001$). Almost all variables contributed to the species effect, but only a few significantly differed between species pairs after Bonferroni corrections (Table S12a), and most species accordingly overlap on the PCAs (Fig. 10A). Yet, some relevant differences are worth noting: the parotoid glands are shorter and narrower in *B. baturae* compared to almost all other species. The Cyprian endemic *B. cypriensis* sp. nov. differs from its close relatives of the *B. viridis* group by narrower parotoids, longer secondary shanks and a generally smaller body size, although only a single population (the type locality) was analyzed.

Body size (snout-vent length, SVL) varied non-randomly across the *Bufotes* radiation (Fig. 10B). Combining our measurements with published averages from hundreds of populations/sample sets, we confirm that species are generally bigger in the *B. viridis* than the *B. latastii* group, while the hybrid taxa have intermediate size: this classification is significant in a Tukey test also accounting for sex ($P < 0.001$ for all three pairwise comparisons). Comparisons between each pair of species are provided in Table S12b.

Fig. 10. Morphometric comparisons between *Bufotes* species; (A) PCA on 16 variables (corrected by SVL), separately for females (F) and males (M); (B) Violin plots of average body sizes (SVL), combining own and published data, arranged along the species tree (hybrid taxa in the middle). Symbol shapes refer to ploidy (2n: circles; 3n: triangles, 4n: rectangles).

3.3. Species distribution modelling

The MaxEnt models received robust evaluation metrics, i.e. test AUCs averaged 0.97 (0.89–1.0), testifying of very good fits. AUC scores and relative contributions of each variable are shown in Table S13. The occurrence data used to build the models, assigned to the corresponding species, is displayed in Fig. S5a.

In the Western Palearctic, the analyses predicted suitable LGM conditions over wide ranges for most species except *B. balearicus*, potentially representing extensive glacial refugia (Fig. S5b). In Central Asia, lowland diploids (*B. perrini* sp. nov. and *B. turanensis*) were supposedly confined to Hindu Kush valleys and what is now the Karakum desert, south of the Aral Sea, while all polyploids (except *B. baturae*) may have expanded over much wider geographic areas, largely overlapping between species (Fig. S5c). The currently disrupted ranges of *B. pseudoraddei* in Pakistan/Afghanistan and India/China (*zamdaensis*) were presumably connected during the LGM. Finally, conditions were mild in some regions of Central Asia for *B. latastii*, and as far north as Afghanistan for *B. surdus*.

3.4. Taxonomic analyses

3.4.1. Identity of B. turanensis

Microsatellite genotypes of the *B. turanensis* type series all matched those published from Shaartuz, Tajikistan (purple diploid lineage, considered as *B. shaartusiensis* since Litvinchuk et al., 2011), rather than those from N-Kyrgyzstan (brown diploid lineage, considered as *B. turanensis* since Stöck et al., 2006). This is illustrated by both the PCA and STRUCTURE analyses, which unambiguously recovered these two lineages as distinct genetic clusters (Fig. 11). STRUCTURE analyses with $K > 2$ did not yield any additional structure.

The circular mitochondrial genome assembly of the holotype MTD 11195 consists of 17,225 bp with a GC content of 40%. It is composed of two ribosomal RNA genes, 22 transfer RNA genes, and 13 protein-coding genes, overall showing an architecture typical of Neobatrachia. The extracted CR and 16S sequences match haplotypes TUR.N06 and TU08, respectively, diagnostic of the purple diploid lineage. Based on a shorter alignment (~200 bp), the nine mitotyped paratypes also fell into this clade.

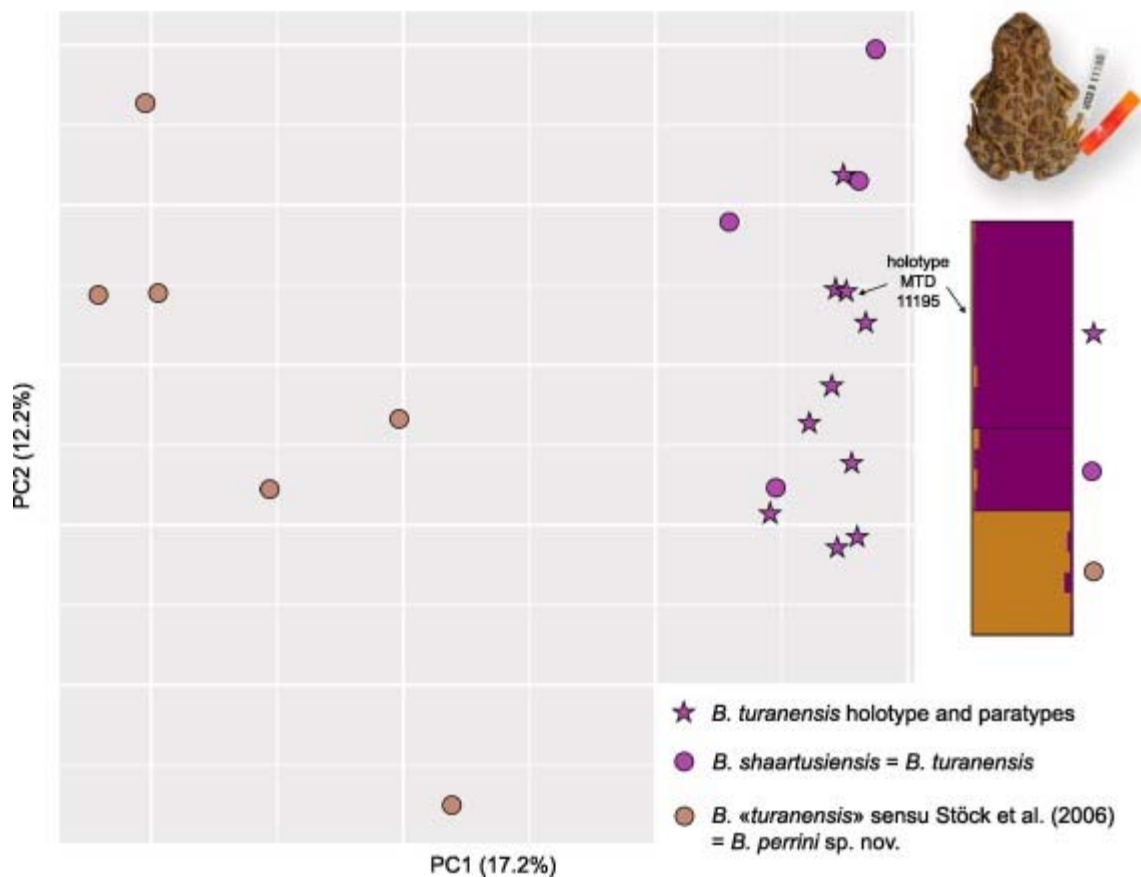Consequently, the nomen *B. turanensis* unambiguously applies to the Amudaryan purple lineage.

Fig. 11. PCA and STRUCTURE assignment probabilities of microsatellites genotyped in the type series of *B. turanensis* (purple stars), and published genotypes from Shaartuz, Tajikistan (topotypes of *B. shaartusiensis*, purple circles) and Bishkek, Kyrgyzstan (considered as *B. turanensis* by Stöck et al., 2006 and subsequent work; brown circles). These analyses indicate that *B. turanensis* and *B. shaartusiensis* are synonyms, and that the brown lineage (*B. turanensis* sensu Stöck) is a different taxon, described here as *B. perrini* sp. nov. Photo credit: RE (holotype of *B. turanensis*). (For interpretation of the references to color in this figure legend, the reader is referred to the web version of this article.)

3.4.2. Distributions and type localities

We provide a fine-scale up-to-date distribution map of the *Bufotes* radiation, with the type localities of valid taxa and those from junior synonyms recently used (Fig. 12). This clarifies range limits and the appropriate nomen for each of them. Details on available names and their junior synonyms are provided in Table S14.
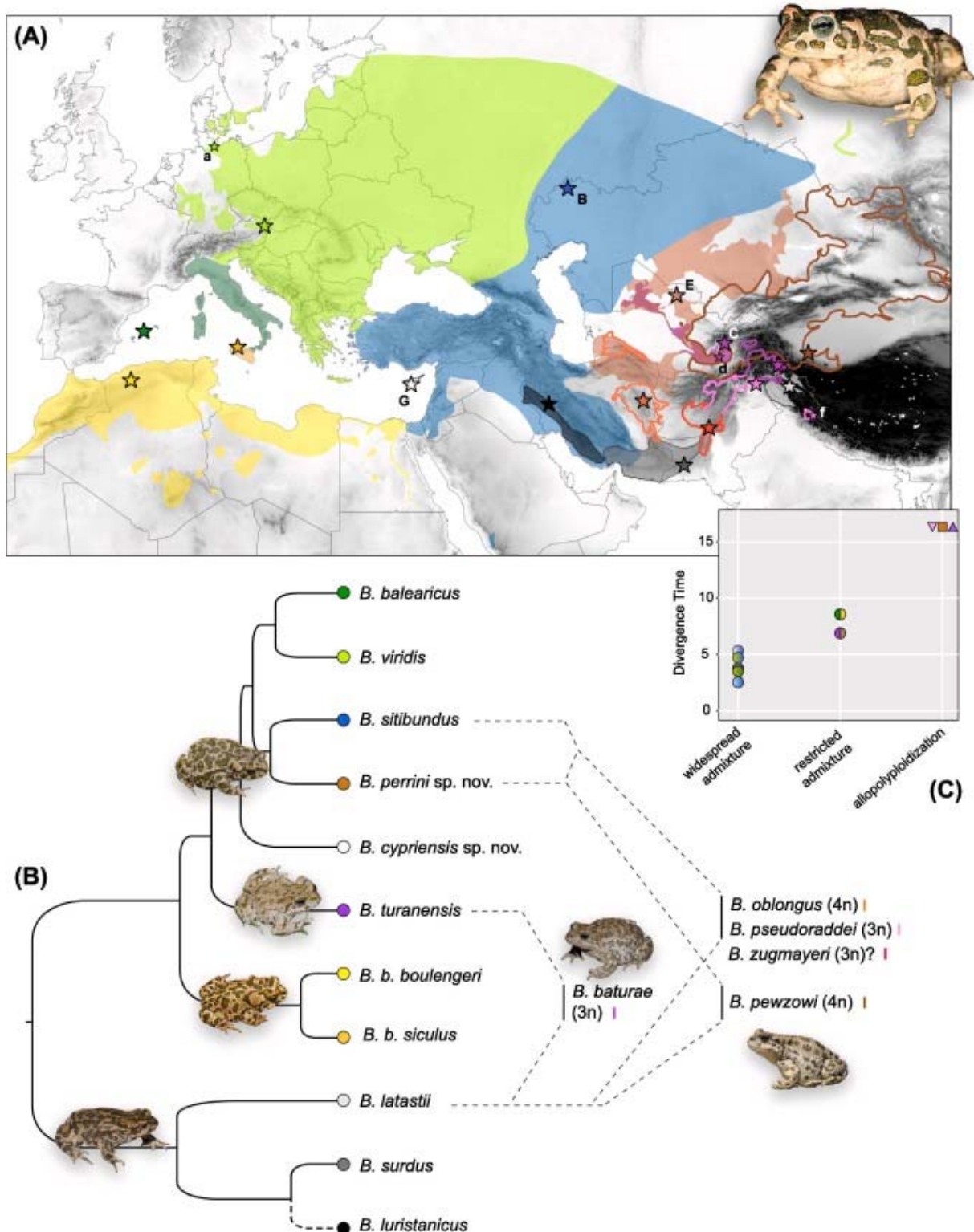
Fig. 12. (A) Range limits of all known *Bufotes* taxa, based on molecular, genome size and occurrence data, adjusted from recent distribution literature (national and regional atlases, Table S8). Diploids are shown in plain colors and allopolyploids in outlines. Type localities of proper taxa are shown in large stars and capital letters (small stars and lower-case letters: recently-used junior synonyms); a: *B. variabilis* (Pallas, 1769), junior synonym of *B. viridis* (Laurenti, 1768); B: *B. sitibundus* (Pallas, 1771), the oldest nomen available for the blue diploid lineage; C: *B. turanensis* (Hemmer et al., 1978), the oldest nomen applying to the purple diploid lineage; d: *B. shaartusiensis* (Pisanets et al., 1996), junior synonym of *B. turanensis*; E: *B. perrini* sp. nov., the newly-described brown diploid lineage; f: *B.*

zamdaensis (Fei et al., 1999), junior synonym of *B. pseudoraddei* (Mertens, 1971); G: *B. cypriensis* sp. nov., the newly-described Cyprian lineage. (B) Species tree of all diploid taxa and the hybridization events that led to known allopolyploids. (C) Categorized outcomes of secondary contacts against divergence time. Photo credit: CD (*B. viridis*, top-right corner), DJ (*B. latastii*, *B. boulengeri*, *B. turanensis*, *B. sitibundus*, *B. baturae*, *B. pewzowi*, on the tree). (For interpretation of the references to color in this figure legend, the reader is referred to the web version of this article)

4. Discussion

By integrating a rich blend of genetic and phenotypic analyses, we dissected and mapped the diversity and distribution of the entire *Bufotes* radiation, namely fifteen Eurasian species now known to science, including ten diploids and five allopolyploids. We gained new insights into their complex evolutionary relationships and hybridization history, and clarified their taxonomy.

4.1. Cyto-nuclear discordance as a hallmark of dynamic phylogeography

4.1.1. Anatolian mtDNA on a European tour

Misled by mitochondrial distributions (Fig. 6), Stöck et al. (2006) speculated on a putative mosaic of *B. viridis* and *B. sitibundus* populations in Central and Northern Europe (the latter as *B. variabilis*, but see Section 4.3.1). In contrast, only *B. viridis* was identified across these ranges from our genome size and RAD data. The widespread occurrence of *B. sitibundus* mtDNA most likely stems from mitochondrial capture during post-glacial recolonizations: *B. sitibundus* and *B. viridis* hybridized at range margins and the mtDNA of the former then surfed on the expansion wave of the latter, thousands of kilometers away. Signals of expansions are evident from the *B. sitibundus* mtDNA clade (see the demographic analyses in Stöck et al., 2006), for which a single CR haplotype (SIT12) was fixed throughout most of Europe. In contrast, and although LGM conditions were not necessarily hostile (Fig. S5b), the alternative scenario for a northern refugium of *B. sitibundus*, subsequently invaded by *B. viridis*, is less likely as these populations should now form a hybrid swarm and host refugial *B. sitibundus* diversity. Thus, this remarkable case adds empirical support that a single range expansion from a genetically-rich source can create misleading phylogeographic patterns, mimicking a segregation of clades of different origins (Excoffier et al., 2009).

Instead, the range margins between *B. viridis* and *B. sitibundus* actually extend across W-Anatolia and the Caspian depression (between the Ural Mountains and the Caucasus), where it broadly follows the Volga River (see the detailed accounts by Faizulin et al., 2018). In their microsatellite analysis of the Aegean region, what Dufresnes et al. (2018a) interpreted as a wide, panmictic *B. viridis*/*sitibundus* hybrid zone across continental Greece rather corresponds to isolation by distance among refugial *B. viridis* populations. Note that the origin of the Siberian isolate of *B. viridis* along the Ob River (vr9) may stem from a human introduction, given that *B. viridis* is absent from adjacent regions (Fig. 12, Fig. S5a), and that invasive *Pelophylax* were also reported in the area (Yakovlev 1987). Finally, our nuclear data also confirmed the independent history of populations from the Adriatic coast, a Pleistocene shelter for many terrestrial vertebrates, especially amphibians (e.g. Dufresnes et al., 2013).

4.1.2. Conflicts in the Middle-East

Most Middle-Eastern amphibians diversified across Asia Minor (e.g. *Hyla orientalis*, Dufresnes et al., 2016), the Caucasus (e.g. *Lissotriton lantzi*, Pabijan et al., 2017) and Hyrcania (e.g. *Rana pseudodalmatina*, Najibzadeh et al., 2017). In *B. sitibundus* however, the lack of nuclear differentiation throughout these regions, despite co-occurrence of deep mitochondrial clades (see also Özdemir et al., 2014) rather indicates episodic isolation followed by lineage fusion, to the point that little phylogeographic structure remains (Fig. 3). The only exception, a young Levantine divergence, is facing a similar fate, given the extensive admixture with Anatolian alleles along the Dead Sea Rift (Fig. 3).

In line with our LGM predictions (Fig. S5b), these melting pots of genetic diversity argue for an unusual connectivity across the Middle-East throughout the Pleistocene climatic fluctuations, as only seen in dry-adapted amphibians (e.g. *Pelobates syriacus*, Dufresnes et al., 2019b). It is best illustrated by our Saudi Arabian locality st18, an isolate that persists ~1500 km away from the Levantine ranges (outside the Palearctic), but did not evolve significant genetic divergence, suggesting dispersal corridors across the Arabian Peninsula in the recent past. In comparison, populations from the same regions diverged since the Pliocene in the tree frog *Hyla felixarabica* (Gvoždík et al., 2010, Dufresnes et al., 2018b), and unlike green toads, that clade barely admixes with its sister taxon *H. savignyi* along the Dead Sea Rift (Dufresnes et al., 2019d).

The diploids found in NE-Iran also feature contrasting mitochondrial *vs* nuclear diversity, as they carry Pleistocene-diverged *B. perrini* sp. nov. mtDNA but faced rampant introgression by *B. sitibundus*, leading to a 3.5% reduction in genome size. We hypothesize that such events predate the formation of polyploid hybrids, which would account for the *B. sitibundus* alleles inherited by the allotriploid *B. pseudoraddei* (Fig. 4), and for the smaller genome size of the allotetraploid *B. oblongus* compared to its eastern counterpart *B. pewzowi* (parented by "pure" *B. perrini* sp. nov.; Fig. 4). Given their putatively old admixture, the diploid toads from NE-Iran/SW-Turkmenistan may become a cryptic homoploid hybrid taxon (Rieseberg, 1997). Such form of hybrid speciation is rare as homoploid hybrids are often replaced quickly by their ancestors, due to weak reproductive barriers and fluctuating range shifts (Chapman and Burke, 2007). The present exception may stem from its temporary geographic isolation, i.e. by the Karakum and Kavir deserts, which offer protection against gene flow from *B. perrini* sp. nov. and *B. sitibundus*, respectively. The modern Aeolian dune systems of the Karakum desert formed as recently as the Quaternary, after Mio-Pliocene tectonic activities and marine incursions finally ceased (Atamuradov, 1994), and since promoted a major phylogeographic break for Central Asia (Graham et al., 2012).

4.1.3. Complete mitochondrial replacement

No less than three species of green toads had their mitochondrial genomes fully replaced through past hybridization. First, we confirmed that the Iranian *B. luristanicus* – the sister-species of *B. surdus* according to Betto-Colliard et al. (2018) and our genome-size data – has fixed an mtDNA related to the *B. viridis* group, as previously reported (Stöck et al., 2006). Considering the strong divergence of its mitotypes, the original hybridization event may date back to the Miocene (Fig. 6), probably involving a maternal ancestor from the European clade and a paternal ancestor from the *B. surdus*/*luristanicus* branch.

Second, we show that the Hindu Kush triploids *B. pseudoraddei* (*B. perrini* sp. nov. × *B. latastii*) and *B. baturae* (*B. turanensis* × *B. latastii*) have contrasted nuclear ancestries, despite that both share mtDNA derived from the *B. turanensis* matriline. This implies two possible scenarios: (i) the maternal ancestor of *B. pseudoraddei* originated from an admixed population (e.g. *B. perrini* sp. nov. carrying *B. turanensis* mtDNA), or (ii) *B. pseudoraddei* lost its original *B. perrini* sp. nov. mtDNA by ancient mitochondrial introgression with *B. turanensis*. Hybridization with the parapatric *B. baturae* would not explain the discordance since this hybrid species arose after the presumed mitochondrial capture (Fig. 6). It is indeed plausible that *B. pseudoraddei* once extended within the ranges of *B. turanensis* and *B. perrini* sp. nov. during the Quaternary, as shown by the LGM predictions.

Third, we present a newly discovered lineage endemic to Cyprus, considered with species level due to its early branching in the nuclear phylogeny, consistent with the end of the Messinian Salinity Crisis. Described herein as *B. cypriensis* sp. nov. (see Section 4.3.4), this taxon adds to a short list of vertebrates unique to the island (e.g. Dubey et al., 2007), where it becomes the second endemic amphibian after the water frog *Pelophylax cypriensis*, also of Messinian origin (Plötner et al., 2012, GM unpublished data). Interestingly, both faced introgression by their Anatolian counterparts (*B. sitibundus* and *P.* cf. *bedriagae*, respectively), indicative of recent land bridges, rafting, drifting and/or human translocations from the continent (Plötner et al., 2015). Green toads tolerate water salinity (to some extent) and are prone to post-Messinian over-sea dispersal to offshore islands, as seen in Crete (*B. viridis* from Peloponnese, and/or *B. sitibundus* from Anatolia; Dufresnes et al., 2018a), Sicily (*B. boulengeri* from N-Africa; Stöck et al., 2008) and the Tyrrhenian and Balearic archipelagos (*B. balearicus* from Italy; Stöck et al., 2006). In Cyprus, this secondary contact led to the complete loss of *B. cypriensis* sp. nov. mtDNA, and insular toads now all bear undifferentiated haplotypes from the Anatolian colonizer *B. sitibundus*.

4.1.4. On causes of discordances and the super-cryptic species concept

With 20% of species entirely lacking a genuine mtDNA (3/15), *Bufotes* may very well hold the record for the highest rate of species-wide mitochondrial capture within a single radiation. Examples of complete mtDNA replacement are found among the whole animal kingdom, but usually represent isolated cases, scarcely seen in mammals (Phuong et al., 2017), fishes (Willis et al., 2014), reptiles (Rabosky et al., 2009), amphibians (Zieliński et al., 2013) and insects (Linnen and Farrell, 2007). The usual suspects include negative (cyto-nuclear incompatibilities) and positive selection (adaptive introgression), sex-biased dispersal, and drift (reviewed in Toews and Brelsford, 2012, Bonnet et al., 2017). While we can only speculate on the relative contributions of these forces in *Bufotes*, several observations should be pointed out. First, the numerous combinations of nuclear and mitochondrial backgrounds across the radiation tend to indicate little selection of either form. Second, whether dispersal is sex-biased in *Bufotes* remains an open question (Trochet et al., 2014), and would actually lead to contradictory conclusions here. For instance, the cases involving *B. sitibundus* are consistent with either female-biased (e.g. its mtDNA colonizing Europe and Cyprus) or male-biased dispersal (e.g. spread of nuclear alleles but not mtDNA in western *B. perrini* sp. nov.). Instead, we argue that demographic factors linked to the instability of *Bufotes* ranges over time, their impressive dispersal capabilities (up to 10 km/year, Trochet et al., 2014) and colonizing efficiency (notably due to their preferences for ephemeral water bodies), combined with a propensity to hybridize upon secondary contacts, make more parsimonious explanations. Range instability was flagged as a major cause of cyto-nuclear discordance in other terrestrial vertebrates (e.g. Phuong et al., 2017). The extent of discordances may be paralleled with the extent of species ranges: the three

taxa that fixed a foreign mtDNA are nowadays highly-localized (Cyprus, SW-Iran, Hindu Kush) and have presumably faced strong drift during Quaternary range shrinkage; in contrast, the mitotypes of more widely distributed taxa were not entirely replaced (e.g. *B. viridis* in Europe). Of course, ranges may have been larger at the time of the mitochondrial capture, given their strong variation during the Quaternary (Fig. S5b–c).

Fortunately for biologists, most taxa known to carry exogenous mtDNA can usually be identified by other features, and/or the hybridization events are old enough so mitochondrial genes re-evolve diagnostic polymorphisms, e.g. *B. luristanicus* and *B. pseudoraddei*. Yet and despite some biometric peculiarities (see Section 4.3.4), here *B. cypriensis* sp. nov. could only be revealed by its nuclear content, i.e. genome size and nuclear SNPs. This special case calls to extend the cryptic species concept to "super-cryptic species", i.e. cryptic species that further lack mitochondrial differentiation. Such situation seriously complicates biodiversity assessments, both because these taxa are overlooked in traditional phylogeographic surveys (e.g. Stöck et al., 2006 did analyze toads from Cyprus), and since their monitoring cannot rely on mtDNA-based barcoding approaches, such as those used in environmental DNA surveys.

The hidden presence of super-cryptic species among otherwise well-documented radiations could actually be a rule rather than an exception. First, cryptic species are increasingly documented worldwide (Coates et al., 2018), but since they rarely feature enough reproductive isolation to become impermeable to gene flow, their recurrent hybridization at range margins creates conditions for frequent mitochondrial capture. Second, the nuclear analyses included in phylogeographic surveys have preferentially aimed at confirming mitochondrial divergences (rarely the other way around), and were thus inherently biased in terms of sampling scheme (e.g. dictated by known mtDNA lineages) and interpretation of the variation observed (e.g. claims of ancestral polymorphism). Furthermore, the nuclear tools used in many phylogeographies (intron markers) may fail to provide a resolution sufficient to resolve recent diversifications (e.g. Dufresnes et al., 2018b), as seen here compared to previous *Bufotes* work (Dufresnes et al., 2018a, Betto-Colliard et al., 2018). Therefore, while the last decades of modern genetics have boosted the discovery of cryptic species, the genomic era may very well initiate a golden age for super-cryptic ones.

4.2. Reticulate evolution of *Bufotes*

4.2.1. Allopolyploid formation

Since the discovery of polyploid green toads (Mazik et al., 1976), multiple studies have gathered complementary evidence towards an understanding of their origin (Mezhzherin and Pisanets, 1995, Betto-Colliard et al., 2015, Betto-Colliard et al., 2018) and reproductive systems (Stöck et al., 2002, Stöck et al., 2005, Stöck et al., 2010). In the wake of recent efforts (Betto-Colliard et al., 2018), we present the first species-level identification for three allopolyploids (summarized in Table 1): (i) the triploid *B. baturae*, as ♂ *B. latastii* × ♀ *B. turanensis*; (ii) the triploid *B. pseudoraddei* (and its synonym *B. zamdaensis*), as ♂ *B. latastii* × ♀ *B. perrini* sp. nov. (western clade); and (iii) the tetraploid *B. pewzowi* as ♂ *B. latastii* × ♀ *B. perrini* sp. nov. (eastern clade). In addition, genome size and mtDNA data leave little doubt for a recent origin of the tetraploid *B. oblongus* as ♂ *B. latastii* × ♀ *B. perrini* sp. nov. (western clade). *Bufotes oblongus* is accordingly the only polyploid with paternal intron sequences closely matching *B. latastii* (although not exclusively, Betto-Colliard et al., 2018). Only the case of the triploid *B. zugmayeri* remains puzzling. Given its nuclear relatedness with *B. pseudoraddei* (on both parental sides, Betto-Colliard et al., 2018), we hypothesize for a similar origin (♂ *B. latastii* × ♀

B. perrini sp. nov.), yet followed by an independent evolutionary trajectory, as seen from its differently balanced chromosomal sets (Table 1) and unrelated mtDNA. Last, we note that Betto-Colliard et al. (2018) misconcluded that *B. pseudoraddei* and *B. zugmayeri* descend from *B. turanensis* (as "*B. shaartusiensis*"), which was not supported by their data.

Table 1. Putative origin of the five *Bufotes* allopolyploid hybrid taxa (see also Fig. 12). Chromosomal balance is taken from Betto-Colliard et al. (2018) and references therein. L: *B. latastii*; T: *B. turanensis*; P: *B. perrini* sp. nov.; Pˢ: *B. perrini* sp. nov. introgressed by *B. sitibundus*.

Hybrid taxon	Ploidy	paternal ancestor	maternal ancestor	Balance	mtDNA
B. baturae	3n	*B. latastii*	*B. turanensis*	LLT	cf. *turanensis*
B. pseudoraddei	3n	*B. latastii*	*B. perrini* sp. nov. (west)	LP^{s}P^s	cf. *turanensis*
B. zugmayeri	3n	*B. latastii?*	*B. perrini* sp. nov. (west)?	LLP?	cf. *perrini* sp. nov. (east)
B. pewzowi	4n	*B. latastii*	*B. perrini* sp. nov. (east)	LLPP	cf. *perrini* sp. nov. (east)
B. oblongus	4n	*B. latastii?*	*B. perrini* sp. nov. (west)	LLP^{s}P^s	cf. *perrini* sp. nov. (west)

Altogether, two pairs of genomes thus appear diverged yet compatible enough to enable polyploid formation (*B. latastii*/*B. turanensis* and *B. latastii*/*B. perrini* sp. nov.), thus involving the three diploid taxa present across Central Asia. Their compatibility further seems irrespective of ploidy background, chromosome balance or putative clonal divergence (in unbalanced triploids), given that most combinations are represented (Table 1) and occasionally interbreed, i.e. *B. pewzowi* (4n) × *B. baturae* (3n) in the Pamirs (Fig. S4), *B. pewzowi* (4n) × *B. turanensis* (2n) in W-Tajikistan (Fig. S4), 3n sp. in Iran (potentially *B. perrini* sp. nov. (2n) × *B. oblongus* (4n) crosses; Litvinchuk et al., 2018) and in Kyrgyzstan (*B. perrini* sp. nov. (2n) × *B. pewzowi* (4n); Stöck et al., 2010). This remarkable genomic plasticity, combined with the dynamic ranges of green toads in Central Asia, has boosted the diversity of hybrid taxa during the Quaternary climatic fluctuations. Given the mtDNA divergences and assuming hybrids descend from the extant populations sequenced, the "hybrid speciation continuum" of *Bufotes* spans from the middle-Pleistocene (*B. pseudoraddei*, *B. pewzowi*, southern *B. oblongus*) to just a few ice ages ago (*B. baturae*, northern *B. oblongus*, undescribed 4n sp. from Bolshoi Balkhan, 3n sp. from Iran), emphasizing the recurrent secondary contacts between diploid ancestors.

Yet, the parental genomes contributed asymmetrically to the hybrid taxa: all events involved maternal ancestors from the *B. viridis* group and a paternal ancestor from the *B. latastii* complex (Betto-Colliard et al., 2018). The directionality of crosses is further seen in 3n sp. triploids from Iran and Kyrgyzstan, both bearing *B. perrini* sp. nov. matrilines (Fig. 6; see also Stöck et al., 2010). Biased paternal *vs* maternal donors are commonly observed in interspecies crosses, including homoploid hybrid taxa throughout the plant (e.g. Tiffin et al., 2001) and animal kingdoms (e.g. Presgraves, 2002). As reviewed by Betto-Colliard et al. (2018), some allopolyploids do show asymmetry in vertebrates, especially on the maternal side (e.g. the unisexual *Ambystoma* salamanders, Bi and Bogart, 2013; the hybrid fish complexes *Cobitis* and *Squalius alburnoides;* Janko et al., 2012, Morgado-Santos et al., 2016), while others rarely do so (e.g. *Xenopus* clawed frogs, Evans et al., 2015).

Asymmetric crossbreeding should reflect pre- and/or post-zygotic isolation between the diverged parents of hybrid species. In this context, we found relevant differences between the

two *Bufotes* groups in terms of breeding calls (Fig. 8) and body size (Fig. 10), two potential determinants of mate choice in anurans. In particular, the direction of crosses is consistent with male preferences for the large females of the *B. viridis* group, a pattern reminiscent of the *Pelophylax* water frogs complex, where the hybridogen *P. esculentus* is preferentially parented by small *P. lessonae* males choosing the large *P. ridibundus* females (Christiansen, 2009, but see Plötner et al., 2008). Given the profound genetic divergence between the segregating genomes, asymmetric post-zygotic incompatibilities are also expected from uniparentally-transmitted genetic elements such as mitochondria, sex chromosomes, or epigenetic factors (Darwin's corollary to Haldane's rule), as empirically evidenced from crossing experiments in toads (Malone and Fontenot, 2008, Brandvain et al., 2015). Bufonids feature labile, mostly homomorphic sex chromosomes (but not exclusively, e.g. Skorinov et al., 2018), shown to be male-heterogametic in the *B. viridis* group (Stöck et al., 2013). The observed asymmetry would thus be in line with lesser X-Y differentiation in *B. latastii*, in turn reducing large-X effects in hybrid crosses fathered by this species, compared to reciprocal crosses. Following recent advances linking sex determination to speciation in bufonids (Gerchen et al., 2018), this hypothesis could be tested by examining sex-chromosome evolution across the entire *Bufotes* radiation.

Once viable polyploid hybrids were formed, their intermediate breeding calls may have promoted sudden pre-mating isolation from their parental ancestors, in turn precipitating speciation events (for a similar case in birds, see Lamichhaney et al., 2018). Accounting for temperature, Stöck (1998) measured slower trills in tetraploids (*B. oblongus*/*B. pewzowi*) compared to Central Asian diploids (*B. perrini* sp. nov.), in accordance with our results. Ploidy level also affects release calls of green toads, under laboratory conditions (Guignard et al., 2012). Ecological differences could have further contributed: polyploids were predicted to occupy transgressive ecological niches (Litvinchuk et al., 2011, Ficetola and Stock, 2016), allowing them to thrive across environments left vacant by diploids during the Pleistocene climatic fluctuations. In Caucasian vipers, a similar mechanism was proposed for the maintenance of hybrid taxa, which occupy anthropogenic habitats, while their ecologically distinct parental species do not (Zinenko et al., 2016). In *Bufotes*, differing ecological preferences may leave physiological signatures. For instance, as the primary defense mechanism, toad poison should evolve in respect to predator assemblages. In polyploid hybrids, the toxin composition was accordingly not intermediate to their respective ancestors, but broadly clustered with the parent sharing putatively similar habitats, i.e. the mountainous *B. baturae*/*pseudoraddei* with *B. latastii*, and the cosmopolitan *B. pewzowi* with *B. perrini* sp. nov. (both sampled from the Uzbek lowlands, Table S5). Whether these associations reflect local adaptation and/or other constraints (i.e. a conserved pathway; Újvari et al., 2015) remains an open question. Altogether, the remarkable diversity of diploid and polyploid green toads across Central Asia provides exciting venues to assess a wide array of genetic, genomic and phenotypic responses to different environmental and ecological conditions.

4.2.2. A discontinuous speciation continuum

Comparative hybrid zone analyses can shed light on the mode and timeframe of allopatric speciation in the wild, which are important aspects of integrative taxonomy (e.g. Dufresnes et al., 2019c). So far only a handful of systems have been comparatively examined at the scale of the radiation (e.g. Arntzen et al., 2014, Dufresnes et al., 2019b, Singhal and Moritz, 2013). With no less than ten interacting lineages, green toads thus make a welcome addition to this short list (Fig. 12). First, Plio-Pleistocene taxa exclusively form large hybrid zones: (i) the intraspecific lineages of *B. sitibundus* across the Levant (massive admixture); (ii) *B. sitibundus* and *B. perrini*

sp. nov. in Iran (massive admixture); (iii) *B. balearicus* and *B. viridis* in NE-Italy (~50 km transition, Dufresnes et al., 2014, Gerchen et al., 2018); (iv) *B. viridis* and *B. sitibundus* in Anatolia/E-Europe (admixture over hundreds of kilometers); and (v) *B. cypriensis* sp. nov. on Cyprus (introgression by *B. sitibundus*). Among these pairs, hybridizability seems rather bounded by geographic (e.g. major rivers, deserts, sea) than reproductive barriers, and appears unrelated to divergence time.

Second, it takes upper-Miocene divergences (7–10 Mya) to grasp clear signs of reproductive isolation: (i) the genetic integrity of *B. turanensis* has remained almost completely intact despite parapatry and even sympatry with both *B. sitibundus* and *B. perrini* sp. nov., perhaps due to its distinct mating calls (Fig. 8); (ii) in Sicily, European (*B. balearicus*) and African toads (*B. boulengeri siculus*) form a tension zone around the Etna, with no contemporary introgression (Colliard et al., 2010, Gerchen et al., 2018).

Third, hybrid speciation can be viewed as the upper-most tip of the speciation continuum, when genomes are too diverged to properly segregate and recombine at meiosis, but for which polyploidy offers an escape route (see Section 4.2.1). Estimated from fossil and geological evidence (Fig. 5), this divergence approximates ~16 My (the *Bufotes* tree root), a figure nearly identical to the split between the *P. lessonae* and *P. ridibundus* genomes of water frogs (GM unpublished data), which similarly co-segregate without recombination in the hybrid context (the homoploid or allotriploid *P. esculentus*, Christiansen, 2009). Following Betto-Colliard et al. (2018), our study is thus in line with the well-supported idea that profound genetic divergence is required to initiate allopolyploidization (Chapman and Burke, 2007), but we object to their unrealistically young dating (~6 My for the tree root; see Section 2.1.5). Beyond this point, green toads may sometimes interbreed with other bufonids (e.g. *B. viridis* × *Bufo bufo*, Duda, 2008; ~36 My of divergence, Portik and Papenfuss, 2015), but these exceptional hybrids are most likely sterile.

Rather than a continuous relationship, patterns of admixture in *Bufotes* support a stepwise accumulation of reproductive isolation with evolutionary divergence, mediated by a threshold below which phylogeographic lineages hybridize relatively freely, but above which genetic introgression becomes the exception rather than the rule. This "discontinuum" implies that barriers to gene flow remain for long inefficient, but grow promptly once initiated, as accumulating Dobzhansky-Muller incompatibilities multiply their effects, and after which speciation is no longer reversible (Dufresnes et al., 2019b, Singhal and Moritz, 2013). Our empirical observations are thus well in line with the "snowball effect" suggested for the build-up of reproductive isolation (Orr, 1995), which so far received mostly theoretical (Orr and Turelli, 2001) and scattered experimental support (Matute et al., 2010, Moyle and Nakazato, 2010). Here, the checkpoint is reached by the end of the Miocene, i.e. between the split of *B. cypriensis* (5.3 My) and the split of *B. turanensis* (~6.9 My). A comparable timeframe is shared by most Palearctic amphibians, e.g. *Hyla* (4–6 My, Dufresnes et al., 2015, Dufresnes et al., 2018b), *Triturus* (4-7 My, Arntzen et al., 2014, Wielstra et al., 2019), *Discoglossus* (3–6 My, Vences et al., 2014, CD unpublished data), while others seem more precocious e.g. *Pelodytes* (~3 My, Diaz-Rodrigues et al., 2017, CD unpublished data) and *Pelobates* (~3 My Dufresnes et al., 2019b). Note that these inferences rely on the molecular clocks applied and the patterns of admixture observed across hybrid zones (which are also affected by neutral factors), and should thus be taken with caution. Nevertheless, they may serve as a benchmark to guide comparative assessments and taxonomic conclusions.

While young phylogeographic lineages may be considered ephemeral if they fuse during secondary contacts (as perhaps ongoing within *B. sitibundus*, see Section 4.1.2), extensive hybridization events act as vector of diversity, here contributing to the unique homoploid nature of western *B. perrini* sp. nov., which, in turn, parented distinctive polyploid taxa. As a consequence, however, cryptic nascent species that still admix with conspecifics become taxonomically controversial in the light of the biological species concept, i.e. most of the *B. viridis* group (see Section 4.3.6). The variability of the "grey zone of speciation" (the divergence window within which deep evolutionary entities can still hybridize; Roux et al., 2016), both in terms of tempo and width, stresses for flexible case-by-case assessments of species delimitation. In the future, universal approaches may benefit from the global perspectives offered by comparative studies integrating additional radiations, and accounting for the varying pace at which speciation progresses in allopatry.

4.3. Taxonomic implications

The present publication, which includes several nomenclatural acts, is registered on ZooBank under the following accession: urn:lsid:zoobank.org:pub:2AC18C16-27C3-4790-9F86-020877B012A6.

4.3.1. Synonymy between B. variabilis and B. viridis

The decade-old nomenclatural controversy regarding green toads inhabiting Anatolia and adjacent regions (blue lineage) is finally resolved. Assuming that the Anatolian clade inhabits northwestern Europe, Stöck et al. (2006) resurrected the nomen *B. variabilis* (Pallas, 1769) with its type locality in Lübeck, northern Germany (close to our locality vr6, Fig. 1; Table S14). Since European populations are only composed of *B. viridis* (Laurenti, 1768), *B. variabilis* shall thus return to its former rank of a junior synonym. Middle Eastern green toads may rather be considered *B. sitibundus* (Pallas, 1771), the oldest available nomen for this nuclear lineage, with type locality as Chaganskoy settlement, Ural River, southern Ural, Kazakhstan (Mertens and Wermuth 1960), located nearby our locality st28 (Fig. 1). Other nomina proposed for this clade are all junior synonyms (Frost 2019; Table S14).

4.3.2. Synonymy between B. zamdaensis and B. pseudoraddei

The triploid *B. zamdaensis* (Fei et al., 1999) is endemic to Sutlej and Spiti valleys at the Indo-Chinese border (Litvinchuk et al., 2012), but is genetically identical to the triploid *B. pseudoraddei* (Mertens, 1971) from Pakistan. These populations most likely correspond to glacial relics that were disconnected during the late-Quaternary, as supported by the LGM distribution and the weak mitochondrial divergence. Therefore, *B. zamdaensis* should be regarded as a junior synonym of *B. pseudoraddei*.

4.3.3. Musical chairs of nomenclature in Central Asia

Using genetic data, we showed that the holotype and paratypes of *B. turanensis* (Hemmer et al., 1978) belong to the purple diploid lineage from the Amudarya River, i.e. the one previously attributed to *B. shaartusiensis* (Pisanets et al., 1996), which then becomes a junior synonym. Potentially misled by the original description of *B. turanensis*, where this species is suggested across the Uzbek and Kazakh plains (Hemmer et al., 1978), Stöck et al. (2006) and subsequent studies have been wrongly applying this nomen to the brown diploid lineage. The nomenclature featured in these studies should thus be disregarded. As it never received an available name,

here we describe the brown lineage as a new species, *B. perrini* sp. nov. (4.3.5). Interestingly, it seems that the type locality of *B. turanensis* (Dushanbe, Tajikistan) is now exclusively inhabited by the tetraploid *B. pewzowi* (see Fig. S4, combining samples from two recent surveys), perhaps indicative of a range shift over the past decades.

4.3.4. Bufotes cypriensis *sp. nov. Litvinchuk, Mazepa, Jablonski, Dufresnes, 2019*

ZooBank accession: urn:lsid:zoobank.org:act:C68F373A-52E1-4BF1-BA6B-5ABD73A37516

Identity and Diagnosis – A diploid species previously considered conspecific to Anatolian green toads due to phenotypic and mitochondrial similarities, and initially assigned to *B. viridis*, later to *B. variabilis* (Stöck et al., 2006; = *B. sitibundus*). This Cyprian endemic initiated divergence when the island was cut off from the mainland at the end of the Messinian Salinity Crisis (5.33 Mya). Today, it outgroups its relatives *B. viridis, B. balearicus, B. sitibundus* and *B. perrini* sp. nov. (Fig. 5), thus warranting a specific taxonomic status. It recently acquired *B. sitibundus* nuclear and mtDNA genes, emphasizing recent connections/introductions from the mainland (see Section 4.1.3).

Based on our type specimens, *B. cypriensis* sp. nov. is the smallest of all W-Palearctic green toads (Fig. 10, Table S9), i.e. 51.0 mm *vs* 61.0–77.7 mm for females, and 54.6 mm *vs* 64.3–75.5 mm for males. Stugren and Tassoula (1987) reported larger, yet still relatively small body sizes (63.7 mm on average, based on 37 unsexed individuals). From our comparisons, *B. cypriensis* differs from several other *Bufotes* members by narrower parotids and shorter secondary shanks (Table S12a), translating into a more stockily-built aspect (Fig. 13A). Males call at 23.0 ± 2.8 pulses/s and 1.39 ± 0.02 kHz, well within the range of other W-Palearctic species (Table S9); a spectrogram and oscillogram are provided on Fig. 13B. Coloration and color patterns were described as very variable (Baier et al., 2009). The clutch and tadpole were not examined.

The karyotype of a male *B. cypriensis* sp. nov. (Finikaria [=Foinikaria], Cyprus, 34.752°N, 33.102°E) is shown in Fig. 13C. The chromosome formula is similar to other diploid *Bufotes*: $2n = 22$ and $NF = 44$, including six large chromosome pairs (each $> 9.7\%$ of the genome) and five small ($<6.1\%$); all are metacentric. The Nucleolus Organizer Region (NOR) lies on the telomeric region of the long arm of pair 5.

Apart from distribution, *B. cypriensis* sp. nov. can be reliably identified from other species by diagnostic substitutions at nuclear DNA: 0.21% of differences with *B. sitibundus*, 0.22% with *B. viridis*, 0.28% with *B. balearicus*, and 0.35% with *B. boulengeri*, based on ~45 kb of RAD tags conserved across the entire *Bufotes* genus. It also exhibits the largest genome size of W-Palearctic *Bufotes*, i.e. 10.51 ± 0.08 pg (Fig. 7, Table S9). Its mitochondrial polymorphism is related to *B. sitibundus* including CR haplotypes SIT32, SIT35-37, SIT42, SIT61 and 16S haplotype ST19 in our samples.

Holotype – ZISP 13849 (field code SL0076), adult female collected by S. N. Litvinchuk on April 25th, 2011 near Finikaria, Cyprus (34.752°N, 33.102°E, 95 m a.s.l.), and deposited at the Zoological Institute, Russian Academy of Science, St. Petersburg, Russia (ZISP); depicted live and post-mortem in Fig. 13A. Measurements are available in Table S6a. Body 51 mm long (snout-vent length), large head with a rounded snout in dorsal view, and abrupt in profile, slightly wider than long. Circular conspicuous tympanum, with distinct annulus, upper margin contacting parotoid. Vomerine teeth visible. Nostrils not protuberant, noticeably closer to each

other than the eyes. Four unwebbed fingers. Legs 44 mm long. Forelegs relatively slender, bearing four fingers. Five long, weakly webbed toes; relative length from inner to outer toes: IV > III > V > II > I. Ventral skin white, granular; dorsal skin smooth with irregular dark spots on grey background (in ethanol); coloration in life creamy white with green camo patterns. ZISP 13849 bears mitochondrial haplotypes SIT35 (CR) and ST19 (16S).
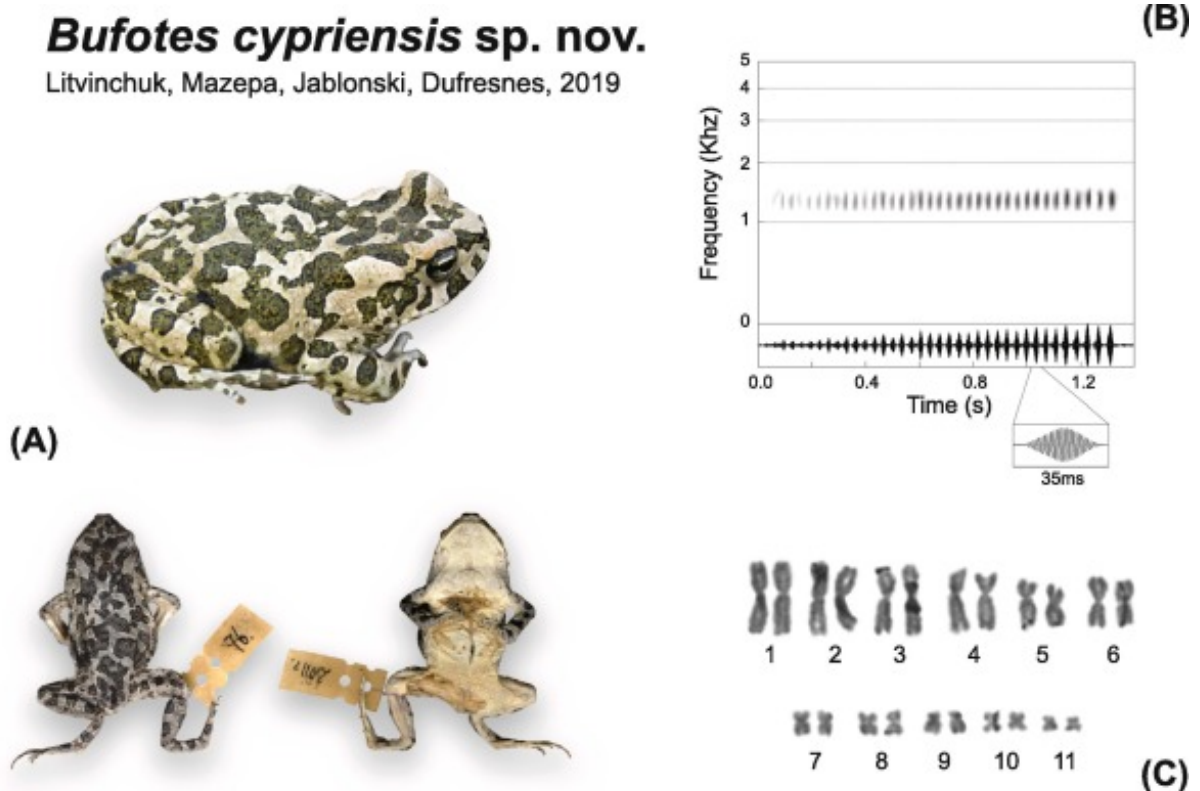

Fig. 13. Description of *Bufotes cypriensis* sp. nov. (A) The holotype ZISP 13849 in life and deposited at the Zoological Institute of the Russian Academy of Science, St Petersburg (ZISP), collected at Finikaria, Cyprus. (B) Spectrogram and oscillogram of a call recorded at Germasogeia, Cyprus. (C) Karyotype of a male from the type locality.

Paratypes – Six paratypes. ZISP 13850-55 (field codes SL0070-75), all males, collected on the same date, by the same collector at the same locality, and also deposited in the ZISP collection. Their mitochondrial haplotypes, measurements, and photos can be found in Tables S1, S6a and Fig. S6, respectively.

Etymology – No bufonid was ever described from Cyprus and so no name was previously available (Table S14). We therefore coin a new name, *Bufotes cypriensis*, which conveys its endemic geographic origin. As a vernacular name, we propose Cyprus Green Toad (English), Кипрская зелёная жаба = Kiprskaya zelyonaya zhaba (Russian), Кіпрська зелена ропуха = Kiprska zelena ropucha (Ukrainian), ropucha cyperská (Slovak), Crapaud Vert de Chypre (French), ropucha kyperská (Czech), Sapo verde de Chipre (Spanish), Κυπριακός Πρασινόφρυνος (Greek).

Distribution and Threats – *B. cypriensis* is endemic to Cyprus, where most populations are distributed along the coasts, from sea level to 700 m a. s. l. (Baier et al., 2009). Fairly common, about 50 sites were known a decade ago (Baier et al., 2009). Nevertheless, its restricted distribution together with the development of touristic activities and extensive use of pesticide

will likely worsen its conservation situation. Pending a formal assessment, we preliminary recommend the IUCN category Vulnerable (VU).

4.3.5. Bufotes perrini *sp. nov. Mazepa, Litvinchuk, Jablonski, Dufresnes, 2019*

ZooBank accession: urn:lsid:zoobank.org:act:8849B1E5-C64D-43E4-B999-7F3E84CA6942

Identity and Diagnosis – A Central Asian diploid of the *B. viridis* group, initially distinguished by the mitochondrial study of Stöck et al. (2006) and since confused with *B. turanensis* (see Section 4.3.3); it thus never received a formal description. Sister clade of *B. sitibundus*, *B. perrini* sp. nov. is granted a specific status given its independent history since the Pliocene.

According to population averages, *B. perrini* sp. nov. is the largest species of the genus i.e. 77.7 ± 7.6 mm for females and 75.5 ± 11.5 mm for males (Fig. 10). Its advertisement calls average 20.4 ± 3.8 pulses/s and 1.27 ± 0.13 kHz; a spectrogram and oscillogram recorded at the type locality are provided in Fig. 14B. Neither bioacoustic nor general biometric features diagnostically differentiate *B. perrini* sp. nov. from its closest relative *B. sitibundus* (Fig. 8, Fig. 9, Fig. 10), with which it widely admixes at range margins, especially in Iran. Yet, it can be readily distinguished on the field from the tetraploids *B. pewzowi*/*oblongus*, by more prominent parotoids, and from the diploid *B. turanensis* by less developed supraorbital crests on the frontoparietal bones (Parchomenko, 2008) and a slower advertisement call (47.8 ± 2.0 pulses/s in *B. turanensis*; Fig. 8). Cranial differences between *B. perrini* sp. nov. and *B. turanensis* are highlighted with CT scanning (Fig. S7), and will need to be compared accounting for ontogenetic changes and sexual dimorphism. The clutch and tadpole were not examined, but egg strings are likely arranged in two rows (as in other diploids), whereas the co-occurring tetraploids *B. pewzowi* and *B. oblongus* lay larger eggs in a single row (Pisanets, 1987).

The karyotype of a male *B. perrini* sp. nov. (Uchquduq, Uzbekistan, 42.117°N, 63.517°N) is shown in Fig. 14C. The chromosome formula is similar to other diploid *Bufotes*: 2n = 22 and NF = 44, including six large chromosome pairs (each >8.4% of the genome) and five small (<5.5%); most chromosomes are metacentric except pairs 4 and 7, which are submetacentric.

At the genetic level, *B. perrini* sp. nov. differs from Central Asian relatives by diagnostic substitutions on nuclear DNA, e.g. 0.12% of differences with *B. sitibundus* and 0.25% with *B. turanensis*, based on ~45 kb of RAD tags conserved across the entire *Bufotes* genus. Its genome size differs from all species inhabiting Central Asia (Tables S9–S10), except in NE-Iran and NW-Turkmenistan where it overlaps with *B. sitibundus* (9.54 ± 0.08 pg *vs* 9.48 ± 0.10 pg). Finally, *B. perrini* sp. nov. features private mtDNA haplotypes at the control region (western populations: PER.W09–12, PER.W14–16; eastern populations: PER.E38–E42, PER.E52, PER.E56) and at 16S (western populations: PR13–14; eastern populations: PR02), distinct from other species and derived polyploids.
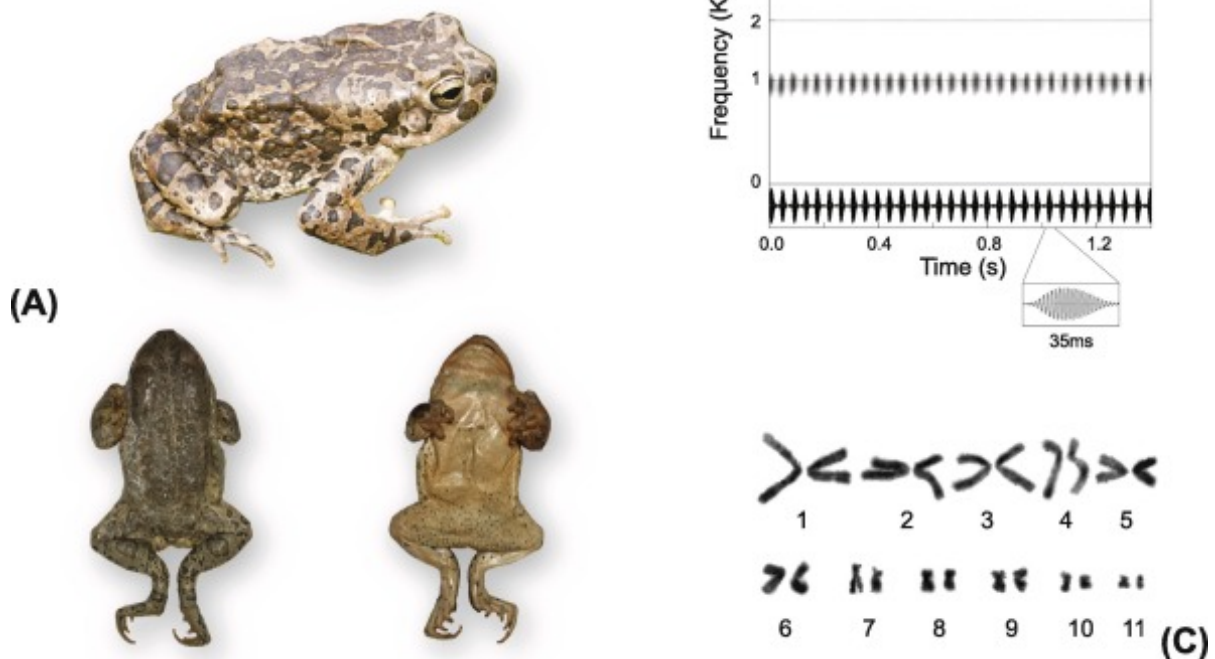
Fig. 14. Description of *B. perrini* sp. nov. (A) A live individual from the type locality, Dzhamanuru spring, Navoi, Uzbekistan, and the holotype MHNG 2782.8, deposited at the Natural History Museum of Geneva (MHNG). (B) Spectrogram and oscillogram of a call recorded at the type locality. (C) Karyotype of male from Uchquduq, Uzbekistan.

Holotype – Male MHNG 2782.8 (field code BV38.1) caught by G. Mazepa on May 5th 2010 in Dzhamanuru spring, Bukantau massif, Navoi, Uzbekistan (42.652°N, 63.315°E), and deposited at the Natural History Museum of Geneva, Geneva, Switzerland (MHNG); depicted post-mortem on Fig. 14A, together with a live topotypic individual. Measurements are available in Table S6a. Large body (SVL = 83.0 mm), broad triangular head, wider (29.8 mm) than long (23.3 mm); snout blunt, with protruding jaw overbite; canthus rostralis rather abrupt; eyes large, interorbital space flat – lateral sides of the frontoparietal bones bear no distinguishable ridges (Fig. S7) – and is slightly larger (6.3 mm) than internarial distance (5.6 mm); nostrils small and round, with narial ring undeveloped, their position marks the abrupt angle between the front and the snout; tympanum oval, distinct, with horizontal diameter (4.0 mm) lesser than half the eye diameter (9.7 mm); tympanum annulus is blurred. Finger length, from shortest to longest: I = II < IV < III; metacarpal tubercles distinct; inner tubercle twice smaller than the outer tubercle; subarticular tubercles rounded, well-developed. Hind limbs relatively short, shank slightly shorter (30.9 mm) than the thigh (31.8 mm); toes moderately long, tips of toes rounded; webbing poorly developed, with webbing formula as I 2 – 2 II 2 – 3 III 3 – 3 IV 3 – 1 V; inner metatarsal tubercle well developed, with length (4.0 mm) 1.6 × the length of toe I (6.4 mm). Dorsum intensively granulated with warts; parotids are very large, twice longer than broad, i.e. left: 23.5 × 10.3 mm and right: 20.4 × 10.3 mm; ventral surface smooth. Color in alcohol: dorsum dark green, almost monotonous; forelimbs and hind limbs with darker spots; ventral surface whitish, marbled with grey and scattered speckles. MHNG 2782.8 bears mitochondrial 16S haplotype PR02.

Paratypes – Three paratypes. ZISP 8945 (male) and ZISP 8946 (female), both collected by I. G. Danilov in September 2006 at Dzharakuduk spring, Bukantau massif, Navoi, Uzbekistan (42.099°N, 62.700°E) and deposited at the Zoological Institute, Russian Academy of Science, St-Petersburg, Russia (ZISP); KUMN Г-1994 (field code BV38.2), female (amplexed with the holotype) collected by G. Mazepa and deposited at the Museum of Nature, V. N. Karazin Kharkiv National University, Kharkiv, Ukraine (KUMN), mummified because of jar leakage. Photos are provided in Fig. S8.

Nomenclature – See Stöck et al. (2001a) and our Table S14 for a detailed account of names coined in the *Bufotes* genus. The diploid taxa described in Central Asia and surrounding regions all represent other species, as follows. ***Bufo cursor* Daudin, 1803**. Types: the specimen illustrated in Lepekhin 1774 (plate XXII, Fig. 6). Type locality: "dans les steppes du Pérémiot près de l'Iaïk" (in the Peremiot steppes near the Ural [=Yaik] River), attributed to "Peremetnoe settlement in Uralsk province, Kazakhstan" by Kuzmin (1999) (51.20°N, 50.82°E, i.e. our locality st27); junior synonym of *B. sitibundus* according to distribution and genetic evidence (see st27 in Fig. 1). ***Bufo viridis* var. *persica* Nikolsky, 1900.** Type locality: restricted to Duz-Ab in E-Kirmano, Iran (~28°N, 58°E) in Stöck et al. (2001a) by lectotype designation; Type(s): lectotype ZISP 2058.3 and seven paralectotypes. Junior synonym of *Bufo surdus* Boulenger, 1891; mentioned here because the nomen *persicus* was earlier quoted to designate *B. viridis* in Steindachner (1867), who refers to Fitzinger, although it is not listed in Fitzinger's catalog (Stöck et al., 2001a). ***Bufo viridis kermanensis* Eiselt, Schmidtler, 1971.** Holotype: NHMW 19647.1. Type locality: Kerman city, Kerman Province, Iran. A diploid form (Stöck et al., 2001a), junior synonym of *B. sitibundus* according to distribution and genetic evidence (Stöck et al., 2006). ***Bufo viridis turanensis* Hemmer, Schmidtler, Böhme, 1978**. Types: MTD 11195 (formerly MTDK 11195) (holotype) and 17 paratypes. Type locality: Dushanbe, Tajikistan (38.54°N, 68.85°E); corresponds to the Amudaryan endemic diploid lineage *B. turanensis* (see Section 4.3.3). ***Bufo kavirensis* Andrén, Nilson, 1979**. Holotype: NHMG Ba.ex 1276. Type locality: Cheshmeh-ye Sefied Ab, Iran (34.35°N, 52.53°E). Most likely a diploid form (Stöck et al., 2001a), junior synonym of *B. sitibundus* according to distribution and genetic evidence (Oraie et al., 2018).

In the absence of any available nomen, we hereby provide a new name for this species, *Bufotes perrini*, after Nicolas Perrin, professor emeritus at the University of Lausanne, and the mastermind behind many scientific contributions on *Bufotes* evolution over the past decade. This tribute also marks the first anniversary of his well-deserved retirement. Proposed common names include Perrin's Green Toad (English), Зелена ропуха Перрена = Zelena ropucha Perrena (Ukrainian), Зелёная жаба Перрена = Zelyonaya zhaba Perrena (Russian), ropucha Perrinova (Czech and Slovak), Crapaud Vert de Perrin (French), Sapo verde de Perrin (Spanish), Perrin qurbaqa (Uzbek).

Distribution and Threats – The range of *B. perrini* covers vast areas within Central Asia, from SE-Kazakhstan to the SW-Caspian shores, largely disrupted by the Karakum desert in Turkmenistan (Borkin et al., 2001b, Stöck et al., 2006, Litvinchuk et al., 2018). The eastern lineage is associated to the arid lowlands from the Amu-Darya on the south (Afghanistan and Uzbekistan, where it is sympatric with *B. turanensis*) towards the eastern side of the former Aral Sea (where it meets and hybridizes with *B. sitibundus*), the middle and lower Syr-Darya flow, eastern side of the Turgai depression, the lower Talas and Chu river drainages as well as the Balkhash Lake basin, hybridizing on the east with *B. pewzowi* along the western foothills of the Tian-Shan mountains system (Stöck et al., 2010). The western lineage is found mostly in arid mountainous areas of SW-Turkmenistan and NE-Iran (Khorasan), which it shares with *B.*

oblongus and 3n sp. from Iran (Litvinchuk et al., 2018). Current contact with *B. sitibundus* in Hyrcania and around the Kavir desert is unclear. Despite a wide range, *B. perrini* always occur in low density and might be locally threatened by aridification and landscape use (including pesticide pollution used for cotton production), we preliminary recommend the IUCN category Near Threatened (NT), pending a formal assessment.

4.3.6. Remaining concerns

The Sicilian endemic *B. siculus* was originally described as a species (Stöck et al., 2008), based on mitochondrial divergence from north-African *B. boulengeri* and private alleles at intronic loci. However, the nuclear divergence is relatively weak (estimated to ~2.5 My, Fig. 5), comparable to the shallow intraspecific clades found within *B. viridis* and *B. sitibundus*, and which freely hybridize in the latter (Levantine ranges, Fig. 3). An intraspecific status would thus be more appropriate for the Sicilian lineage and we follow Speybroeck et al. (2010) to consider it a subspecies of *B. boulengeri*, namely *B. boulengeri siculus*. Note that suspicion remains on the availability of the nomen "*siculus*", given that the corresponding description (Stöck et al., 2008) was only issued electronically, and prior to 2011 – see Article 8.5 of the International Code for Zoological Nomenclature (ICZN); whether "numerous identical and durable copies" (Article 8.1) were registered by the authors in parallel is yet to be addressed (P.A. Crochet pers. comm.).

The Adriatic (*B.* cf. *viridis*), N-Iranian/NW-Turkmenian (*B.* cf. *perrini* sp. nov.), and Levant/Saudi Arabian populations (*B.* cf. *sitibundus*) could also be eligible for a subspecific rank, pending additional efforts to clarify their ranges, distinction from their nominal taxa and nomenclatural availability. First, the nomen *Bufo longipes* Fitzinger in Bonaparte, 1840 (as "*Bufo viridis* var.? *Bufo longipes*"), with type locality "Dalmatia" seems available for the Adriatic populations, once the distribution of this isolate will be fine-tuned (present sampling is limited to the northern and southern edges of the Dalmatian coast; Fig. 6). Second, no name was attributed to the homoploid hybrid populations from N-Iran and NW-Turkmenistan (*B.* cf. *perrini*; see Section 4.3.5), but we recommend to extend investigations of their nuclear background (together with the associated tetraploid *B. oblongus*) before taking taxonomic actions. Third, no *Bufotes* populations from the Levant and Saudi Arabia have so far been described. In the past, the nomen "*arabicus*" has been wrongly used to designate these populations (*B. viridis arabicus*, e.g. Stugren and Tassoula 1987), although it corresponds to *Sclerophrys arabicus*. This lineage could thus be a candidate for a formal description, ideally from the southernmost populations.

The poorly-understood distribution, phylogeny and putative hybridization with *B. viridis* had casted doubts on the specific status of *B. sitibundus* (Dufresnes et al., 2018a). As our data shows, *B. sitibundus* and *B. viridis* are not sister clades when considering *B. balearicus* and *B. perrini* (see also Betto-Colliard et al., 2018). Although the argument that all four may then be considered subspecies is receivable (Speybroeck et al., 2010), given their wide hybrid zones (Fig. 12) and shared phenotypes (advertisement calls, morphology, toxin), we choose here to keep them as distinct species given the deep phylogenetic divergence, consistent with the timeframe of speciation in other Palearctic anurans (see Section 4.2.2).

Finally, we outline two additional geographic regions recently studied by Dufresnes et al. (2018a) as potential candidates for further taxonomic changes. First, green toads from the Aegean island of Naxos (Central Cyclades) bear endemic haplotypes at mitochondrial and nuclear genes, as well as peculiar microsatellite profiles (shared with the coastal island of

Ikaria); they may very well represent a separate taxon, pending further analyses. Second, Cretan populations nuclearly differ from the mainland and likely experienced multiple colonization events given their mtDNA diversity; they deserve genomic investigations. Like in Cyprus, off-shore islands that experienced long-term disconnection but occasionally faced oversea dispersal, make prime candidates for super-cryptic differentiation.

5. Conclusions

Combining various approaches, we have provided an extensive update of the phylogeography, evolution, distribution and taxonomy of the *Bufotes* genus, with new insights on the genomic and phenotypic plasticity of the fifteen identified species. We unveiled multiple cyto-nuclear discordances that previously blurred the range limits of widespread taxa, concealed a super-cryptic one, and confounded the origin of hybrid species. Incorporating previous work, we substantiated a stepwise progression of speciation through time and framed the conditions necessary for allopolyploidization. Embracing the genomic age, our framework marks the advent of a new exciting era for evolutionary research in these iconic amphibians.

Appendix A. Supplementary material

The following are the Supplementary data to this article:

Supplementary Figs. S1–S8.

Supplementary Tables S1–S14.

References

Aitchison J. 1982. The statistical-analysis of compositional data. J. R. Stat. Soc. Series B. Stat. Methodol. 44, 139–177.

Arntzen JW, Wielstra B, Wallis GP. 2014. The modality of nine *Triturus* newt hybrid zones assessed with nuclear, mitochondrial and morphological data. Biol. J. Linn. Soc. 113, 604–622.

Atamuradov KI. 1994. Paleogeography of Turkmenistan. Pp. 49-64 in Fet V, Atamuradov KI (Eds). Biogeography and Ecology of Turkmenistan – Kluwer Academic Publishers, Dordrecht, Netherlands.

Baier F, Sparrow DJ, Wiedl H-J. 2009. The amphibians and reptiles of Cyprus. Chimaira edition, Frankfurt am Main, Germany.

Bernt M, Donath A, Jühling F, Externbrink F, Florentz C, Fritzsch G, Pütz J, Middendorf M, Stadler PF. 2013. MITOS: Improved de novo Metazoan Mitochondrial Genome Annotation. Mol. Phylogenet. Evol. 69, 313–319.

Berthier P, Excoffier L, Ruedi M. 2007. Recurrent replacement of mtDNA and cryptic hybridization between two sibling bat species *Myotis myotis* and *Myotis blythii*. Proc. R. Soc. Lond. B. Biol. Sci. 273, 3101–3109.

Betto-Colliard C, Sermier R, Litvinchuk S, Perrin N, Stöck M. 2015. Origin and genome evolution of polyploid green toads in Central Asia: evidence from microsatellite markers. Heredity 114, 300–308.

Betto-Colliard C., Hofmann S., Sermier R., Perrin N., Stock M. 2018. Profound genetic divergence and asymmetric parental genome contributions as hallmarks of hybrid speciation in polyploid toads. Proc. R. Soc. B 285, 20172667.

Bi K, Bogart JP. 2013 Genetic and genomic interactions of animals with different ploidy levels. Cytogen. Genome Res. 140, 117–136.

Bonaparte CLJL. 1840. Amphibia Europaea ad systema nostrum vertebratorum ordinata. Memoria della Reale Accademia delle Scienze di Torino. Serie 2, Tome 2.

Bonnet T, Leblois R, Rousset F, Crochet P-A. 2017. A reassessment of explanations for discordant introgressions of mitochondrial and nuclear genomes. Evolution 71, 2140–218.

Borkin LJ, Litvinchuk SN, Rosanov JM, Milto KD. 2001a. Cryptic speciation in *Pelobates fuscus* (Anura, Pelobatidae): evidence from DNA flow cytometry. Amphibia-Reptilia 22, 387–396.

Borkin LJ, Eremchenko VK, Helfenberger N, Panfilov AM, Rosanov JM. 2001b. On the distribution of diploid, triploid, and tetraploid green toads (*Bufo viridis* complex) in south-eastern Kazakhstan. Russ. J. Herpetol. 8, 45–53.

Bouckaert RR, Drummond AJ. 2017. bModelTest: Bayesian phylogenetic site model averaging and model comparison. BMC Evol. Biol 17, 42.

Bouckaert RR, Heled J. 2014. DensiTree 2: seeing trees through the forest. Retrieved from http://dx.doi.org/10.1101/012401.

Bouckaert R, Heled K., Khünert D., Vaughan T, Wu CH, Xie D, et al. 2014. BEAST 2: A software platform for Bayesian Evolutionary Analysis. PLoS Comput. Biol.10, e1003537.

Brandvain Y, Pauly GB, May M, Turelli M. 2015 Explaining Darwin's corollary to Haldane's Rule: the role of mitonuclear interactions in asymmetric postzygotic isolation among toads. Genetics 197, 743–747.

Brelsford A, Dufresnes C, Perrin N. 2016. High-density sex-specific linkage maps of a European tree frog (*Hyla arborea*) identify the sex chromosome without information on offspring sex. Heredity 116, 177–181.

Buerkle CA, Wolf DE, Rieseberg LH. 2003. The origin and extinction of species through hybridization. Pp. 117–141 in Brigham CA, Schwarz MW (Eds). Population viability in plants. Springer, Berlin/Heidelberg, Germany.

Catchen J, Hohenlohe P, Bassham S, Amores A, Cresko W. 2013. Stacks: an analysis tool set for population genomics. Mol. Ecol. 22, 3124–3140.

Chan KM, Levin SA. 2005. Leaky prezygotic isolation and porous genomes: rapid introgression of maternally inherited DNA. Evolution 59, 720–729.

Chapman MA, Burke JM. 2007 Genetic divergence and hybrid speciation. Evolution 61, 1773–1780

Canestrelli D, Bisconti R, Sacco F, Nascetti G. 2014. What triggers the rising of an intraspecific biodiversity hotspot? Hints from the agile frog. Sci. Rep. 4, 5042.

Castellano S, Rosso A, Doglio S, Giacoma C. 1999. Body size and calling variation in the green toad (*Bufo viridis*). J. Zool., Lond. 248, 83–90.

Christiansen DF. 2009. Gamete types, sex determination and stable equilibria of all-hybrid populations of diploid and triploid edible frogs (*Pelophylax esculentus*). BMC Evol. Biol. 9, 135.

Coates DJ, Byrne M, Moritz C. 2018. Genetic diversity and conservation units: dealing with the speciation-population continuum in the age of genomics. Front. Ecol. Evol 6, 165.

Colliard C, Sicilia A, Turrisi GF, Arculeo M, Perrin N, Stöck M. 2010. Strong reproductive barriers in a narrow hybrid zone of West-Mediterranean green toads (*Bufo viridis* group) with Plio-Pleistocene divergence. BMC Evol. Biol. 10, 232.

Currat M, Ruedi M, Petit RJ, Excoffier L. 2008. The hidden side of invasions: massive introgression by local genes. Evolution 62, 1908–1920.

Csardi G, Nepusz T. 2006. The igraph software package for complex network research. Int. J. Complex Syst. 1695.

Dai C, Wang W, Lei F. 2013. Multilocus phylogeography (mitochondrial, autosomal and Z-chromosomal loci) and genetic consequences of long-distance male dispersal in Black-throated tits (*Aegithalos concinnus*). Heredity 110, 457–465.

Daly JW, Spande TF, Garraffo HM. 2005. Alkaloids from amphibian skin: a tabulation of over eight-hundred compounds. J. Nat. Prod. 68.10, 1556-1575.

Degnan JH, Rosenberg NA. 2009. Gene tree discordance, phylogenetic inference and the multispecies coalescent. Trends Ecol. Evol. 24, 332–340.

Diaz-Rodriguez J, Gehara M, Marquez R, Vences M, Goncalves H, Sequeira F, Martinez-Solano I, Tejedo M. 2017. Integration of molecular, bioacoustical and morphological data reveals two new cryptic species of *Pelodytes* (Anura, Pelodytidae) from the Iberian Peninsula. Zootaxa 4243, 1–41.

Dray S, Dufour A. 2007. The *ade4* package: Implementing the duality diagram for ecologists. J. Stat. Softw. 22, 1–20.

Dubey S, Cosson JF, Magnanou E, Vohralík V, Benda P, Frynta D, Hutterer R, Vogel V, Vogel P. 2007. Mediterranean populations of the lesser white-toothed shrew (*Crocidura suaveolens* group): an unexpected puzzle of Pleistocene survivors and prehistoric introductions. Mol. Ecol. 16, 3438–3452.

Dubey S, Maddelena T, Bonny L, Jeffries DL, Dufresnes C. Population genomics of an exceptional hybridogenetic system of *Pelophylax* water frogs. BMC Evol. Biol. 19, 164.

Duda M. 2008. First record of a natural male hybrid of *Bufo* (*Pseudepidalea*) *viridis* Laurenti, 1768 and *Bufo* (*Bufo*) *bufo* Linneus, 1758 from Austria. Herpetozoa 20, 184–186.

Dufresnes C, Strachinis I, Tzoras E, Litvinchuk SN, Denoël M. 2019c. Call a spade a spade: taxonomy and distribution of *Pelobates*, with description of a new Balkan endemic. ZooKeys, 859, 131-158.

Dufresnes C, Wassef J, Ghali K, Breslford A, Stöck M, Lymberais P, Crnobrnja-Isailovic J, Perrin N. 2013. Conservation phylogeography: does historical diversity contribute to regional vulnerability in European tree frogs (*Hyla arborea*)? Mol. Ecol. 22, 5669–5684.

Dufresnes C, Bonato L, Novarini N, Betto-Colliard C, Perrin N, Stöck M. 2014. Inferring the degree of incipient speciation in secondary contact zones of closely related lineages of Palearctic green toads (*Bufo viridis* group). Heredity 113, 9–20.

Dufresnes C, Brelsford A, Crnobrnja-Isailovic J, Tzankov N, Lymberakis P, Perrin N. 2015. Timeframe of speciation inferred from secondary contact zones in the European tree frog radiation (*Hyla arborea* group). BMC Evol. Biol. 15, 155.

Dufresnes C, Litvinchuk SN, Leuenberger J, Ghali K, Zinenko O, Stöck M, Perrin N. 2016. Evolutionary melting pots: a biodiversity hotspot shaped by ring diversifications around the Black Sea in the Eastern tree frog (*Hyla orientalis*). Mol. Ecol. 25, 4285–4300.

Dufresnes C, Lymberakis P, Kornilios P, Savary R, Perrin N, Stöck M. 2018a. Phylogeography of Aegean green toads (*Bufo viridis* group): continental hybrid swarm vs. insular diversification with discovery of a new island endemic. BMC Evol. Biol. 18, 67.

Dufresnes C, Mazepa G, Jablonski D, Sadek RA, Litvinchuk SN. 2019d. A river runs through it: tree frog genomics supports the Dead Sea Rift as a rare phylogeographic break. Biol. J. Linn. Soc. 128, 130-137.

Dufresnes C, Mazepa G, Rodrigues N, Brelsford A, Litvinchuk SN, Sermier R, Lavanchy G, Betto-Colliard C, Blaser O, Borzée A, Cavoto E, Fabre G, Ghali K, Grossen C, Horn A, Leuenberger J, Phillips BC, Saunders PA, Savary R, Maddalena T, Stöck M, Dubey S, Canestrelli D, Jeffries DL. 2018b. Genomic evidence for cryptic speciation in tree frogs from the Apennine Peninsula, with description of *Hyla perrini* sp. nov. Front. Ecol. Evol. 6, 144.

Dufresnes C, Beddek M, Skorinov DV, Fumagalli L, Perrin N, Crochet P-A, Litvinchuk SN. 2019a. Diversification and speciation in tree frogs from the Maghreb (*Hyla meridionalis sensu lato*), with description of a new African endemic. Mol. Phylogenet. Evol. 134, 291–299.

Dufresnes C, Strachinis I, Suriadna N, Mykytynets G, Cogălniceanu D, Vukov T, Székely P, Vukov T, Arntzen JW, Wielstra B, Lymberakis P, Geffen E, Gafny S, Kumlutaş Y, Ilgaz C, Candan K, Mizsei E, Szabolcs M, Kolenda K, Smirnov N, Géniez P, Lukanov S, Crochet P-A, Dubey S, Perrin N, Litvinchuk SN, Denoël M. 2019b. Phylogeography of a cryptic speciation continuum in Eurasian spadefoot toads (*Pelobates*). Mol. Ecol. 28, 3257-3270.

Earl DA, von Holdt BM. 2012. STRUCTURE HARVESTER: a website and program for visualizing STRUCTURE output and implementing the Evanno method. Conserv. Genet. Resour. 4, 359–361.

Ehl S, Vences M, Veith M. 2019. Reconstructing evolution at the community level: a case study on Mediterranean amphibians. Mol. Phylogenet. Evol. 134, 211-225.

Evans BJ, Carter TF, Greenbaum E, Gvoždík V, Kelley DB, McLaughlin PJ, Pauwels OSG, Portik DM, Stanley EL, Tinsley RC, Tobias ML, Blackburn DC. 2015. Genetics, morphology, advertisement calls, and historical records distinguish six new polyploid species of African Clawed Frog *Xenopus*, Pipidae from West and Central Africa. PLoS ONE 10, e0142823.

Excoffier L, Foll M, Petit RJ. 2009. Genetic consequences of range expansions. Annu. Rev. Ecol. Evol. Syst. 40, 481–501.

Faizulin AI, Svinin AO, Ruchin AB, Skorinov DV, Borkin LJ, Rosanov JM, Kuzovenko AE, Litvinchuk SN. 2018. Distribution and contact zone of two forms of the green toad from the *Bufotes viridis* complex (Anura, Amphibia), differing in genome size, in the Volga region. Curr. Stud. Herpetol. Saratov 18, 35–45.

Ficetola GF, Stock M. 2016. Do hybrid-origin polyploid amphibians occupy transgressive or intermediate ecological niches compared to their diploid ancestors? J. Biogeogr. 43, 703–715.

Frost D. 2019. Amphibian Species of the World: an Online Reference. Version 6.0. American Museum of Natural History, New York, USA (Accessed June 1st 2019). http://research.amnh.org/herpetology/amphibia/index.html.

Garrick RC, Banusiewicz JD, Burgess S, Hyseni C, Symula RE. 2019. Extending phylogeography to account for lineage fusion. J. Biogeogr. 46, 268–278.

Gerchen JF, Dufresnes C, Stöck M. 2018. Introgression across hybrid zones is not mediated by Large X-Effects in green toads with undifferentiated sex chromosomes. Am. Nat. 192, 178–188.

Graham MR, Olah-Hemmings V, Fet V. 2012. Phylogeography of co-distributed dune scorpions identifies the Amu Darya River as a long-standing component of Central Asian biogeography. Zool. Middle East 55, 95–110.

Guignard MS, Büchi L, Gétaz M, Colliard C, Stöck M. Genome size rather than content might affect call properties in toads of three ploidy levels (Anura: Bufonidae: *Bufo viridis* group). Biol. J. Linn. Soc. 105, 584–590.

Gvoždík V, Moravec J, Klütsch C, Kotlik P. 2010. Phylogeography of the Middle Eastern tree frogs (*Hyla*, Hylidae, Amphibia) inferred from nuclear and mitochondrial DNA variation, with a description of a new species. Mol. Phylogenet. Evol. 55, 1146–1166.

Hallatschek O, Nelson DR. 2008. Gene surfing in expanding populations. Theor. Popul. Biol. 73, 158–170.

Hemmer H, Schmidtler JF, Böhme W. 1978. Zur Systematik zentralasiatischer Grünkröten (Bufo viridis-Komplex) (Amphibia, Salentia, Bufonidae). Zool. Abh. Dres. 34, 349–384.

Köhler J, Jansen N, Rodriguez A, Kok PJR, Toledo LF, Emmrich M, Glaw F, Haddad CFB, Rödel M-O, Vences M. 2017. The use of bioacoustics in anuran taxonomy: theory, terminology, methods and recommendations for best practice. Zootaxa 4251, 1–124.

Kuzmin SL. 1999. The amphibians of the former Soviet Union. Pensoft Publisher, Sofia, Bulgaria.

Janko K, Kotusz J, De Gelas K, Slechtova V, Opoldusova Z, Drozd P, Choleva L, Popiołek M, Balaz M. 2012. Dynamic formation of asexual diploid and polyploid lineages: multilocus analysis of *Cobitis* reveals the mechanisms maintaining the diversity of clones. PLoS ONE 79, e45384.

Jin Y, Wo Y, Tong H, Song S, Zhang L, Brown RP. 2018. Evolutionary analysis of mitochondrially encoded proteins of toad-headed lizards, *Phrynocephalus*, along an altitudinal gradient. BMC Genom. 19, 1–11.

Jombart T. 2008. *adegenet*: a R package for the multivariate analysis of genetic markers. Bioinformatics 24, 1403–1405.

Lamichhaney S, Han F, Webster MT, Andersson L, Grant BR, Grant PR. 2018. Rapid hybrid speciation in Darwin's finches. Science 359, 224–228.

Lê S, Josse J, Husson F. 2008. FactoMineR: an R package for multivariate analysis. J. Stat. Softw. 25, 1–18.

Lepekhin II. 1774. Tagebuch der Reise durch verschiedene Provinzen des Russischen Reiches in den Jahren 1768 und 1769. Richterischer Buchhandlung, Altenbourg, Germany.

Linnen CR, Farrell BD. 2007. Mitonuclear discordance is caused by rampant mitochondrial introgression in *Neodiprion* (Hymenoptera: Diprionidae) sawflies. Evolution 61, 1417–1438.

Litvinchuk SN, Mazepa GO, Pasynkova RA, Saidov A, Satorov T, Chikin YA, Shabanov DA, Crottini A, Borkin LJ, Rosanov JM, Stöck M. 2011. Influence of environmental conditions on the distribution of Central Asian green toads with three ploidy levels. J. Zool. Syst. Evol. Res. 49, 233–239.

Litvinchuk SN, Borkin LJ, Skorinov DV, Mazepa GA, Pasynkova RA, Dedukh DV, Krasikova AV, Rosanov JM. 2012. Unusual triploid speciation in green toads *Bufo viridis* group in High-altitude Asia. Pp. 160-165 in Novitskiy RV (Ed). Problems of Herpetology. Minsk, Belarus.

Litvinchuk SN, Skorinov DV, Borkin LJ, Pasynkova RA, Rosanov JM. 2017. Natural triploidy in two Chinese frogs of the genus *Glandirana* (Anura; Ranidae). Russ. J. Herpetol. 24, 235–237.

Litvinchuk SN, Borkin LJ, Mazepa GA, Rosanov JM. 2018. Genome size and distribution of diploid and polyploidy green toads of the genus *Bufotes* in Uzbekistan and Turkmenistan. Pp. 88-101 in Rustamov EA (Ed). Herpetological and Ornithological Research: Current Aspects. Dedicated to the 100th Anniversary of A. K. Rustamov (1917–2005). KMK Scientific Press, Moscow, Russia.

Mallet J, Besansky N, Hahn MW. 2015. How reticulated are species? Bioessays 38, 140–149.

Malone JH, Fontenot BE. 2008. Patterns of reproductive isolation in toads. PLoS ONE 12, e3900.

Matute DR, Butler IA, Turissini DA, Coyne JA. 2010. A test of the snowball theory for the rate of evolution of hybrid incompatibilities. Science 329, 1518–1521.

Mazik E, Kadyrova BK, Toktosunov AT. 1976. Osobennosti kariotipa zelenoi žaby (*Bufo viridis*) v Kirgizii. Zool. Zhurn. 55, 1740–1742.

Mertens R, Wermuth H. 1960. Die Amphibien und Reptilien Europas. Frankfurt am Main, Germany.

Mezhzherin SV, Pisanets EM. 1995. Genetic structure and origin of the tetraploid toad *Bufo danatensis* Pisanetz, 1978 (Amphibia, Bufonidae) from Central Asia: differentiation of geographic forms and genetic relationship between diploid and tetraploid species. Genetika 31, 342–352.

Morgado-Santos M, Carona S, Magalhaes MF, Vicente L, Collares-Pereira MJ. 2016. Reproductive dynamics shapes genomotype composition in an allopolyploid complex. Proc. R Soc. B 283, 20153009.

Moyle LC, Nakazato T. 2010. Hybrid incompatibilities "snowballs" between Solanum species. Science 329, 1521–1523.

Najibzadeh M, Veith M, Gharzi A, Rastegar-Pouyani N, Rastegar-Pouyani E, Kieren S, Pesarakloo A. 2017. Molecular phylogenetic relationships among Anatolian-Hyrcanian brown frog taxa (Ranidae: *Rana*). Amphibia-Reptilia, 38, 339–350.

Ottenburghs J. 2018. Exploring the hybrid speciation continuum in birds. Ecol. Evol. 8, 13027-13034.

Oraie H, Rastegar-Pouyani E, Khosravani A, Adibi MA. 2018. Identical mitochondrial haplotypes of specimens from the type locality of *Bufotes kavirensis* (Andrén & Nilson, 1979) and *B. variabilis* (Pallas, 1769) (Anura: Bufonidae) from Iran. Acta Zool. Bulg. 70, 297–303.

Orr H. 1995. The population genetics of speciation: the evolution of hybrid incompatibilities. Genetics 139, 1805–1813.

Orr HA, Turelli M. 2001. The evolution of postzygotic isolation: accumulating Dobzhansky-Muller incompatibilities. Evolution 55, 1085–1094.

Özdemir N, Gül S, Poyarkov Jr. NA, Kutrup B, Tosunoglu M, Doglio S. 2014. Molecular systematics and phylogeography of *Bufotes variabilis* (syn. *Pseudepidalea variabilis*) (Pallas, 1769) in Turkey. Turk. J. Zool. 38, 412–420.

Pabijan M, Zielinski P, Dudek K, Stuglik M, Babik W. 2017. Isolation and gene flow in a speciation continuum in newts. Mol. Phylogenet. Evol. 116, 1–12.

Padial JM, Miralles A, De la Riva I, Vences M. 2010. The integrative future of taxonomy. Front. Zool. 7, 16.

Paradis E. 2010. *pegas*: an R package for population genetics with an integrated modular approach. Bioinformatics 26, 419–420.

Parchomenko MN. 2008. The variability of osteologycal characters in some Palearctic toads of genus *Bufo* (Amphibia, Anura, Bufonidae). Proc. Ukr. Herpetol. Soc. Kyiv 1, 59–66.

Pfennig KS. 2016. Reinforcement as an initiator of population divergence and speciation. Curr. Zool. 62, 145–154.

Pisanets EM. 1987. Differences in egg clutch between green and Danata toads. Vestn. Zool. 6, 80–81.

Phillips S, Anderson R, Schapire R. 2006. Maximum entropy modeling of species geographic distributions. Ecol. Modell. 190, 231–259.

Phillips SJ, Dudík M. 2008. Modeling of species distributions with Maxent: new extensions and a comprehensive evaluation. Ecography 31, 161–175.

Phuong MA, Bi K, Moritz C. 2017. Range instability leads to cytonuclear discordance in a morphologically cryptic ground squirrel species complex. Mol. Ecol. 26, 4743–4755.

Plötner J, Uzzell T, Beerli P, Spolsky C, Ohst T, Litvinchuk SN, Guex G-D, Reyer H-U, Hotz H. 2008. Widespread unidirectional transfer of mitochondrial DNA: a case in western Palaearctic water frogs. J. Evol. Biol. 21, 668–681.

Plötner J, Baier F, Akin C, Mazepa G, Schreiber R, Beerli P, Litvinchuk SN, Can Bilgin C, Borkin L, Uzzell T. 2012. Genetic data reveal that water frogs of Cyprus (genus *Pelophylax*) are an endemic species of Messinian origin. Zoosyst. Evol. 88, 261–283.

Plötner J, Akin Peksen C, Baier F, Uzzell T, Can Bilgin C. 2015. Genetic evidence for human-mediated introduction of Anatolian water frogs (*Pelophylax* cf. *bedriagae*) to Cyprus (Amphibia: Ranidae). Zool. Middle East 61, 125–132.

Portik DM, Papenfuss TJ. 2015. Historical biogeography resolves the origins of endemic Arabian toad lineages (Anura: Bufonidae): evidence for ancient vicariance and dispersal events with the Horn of Africa and South Asia. BMC Evol. Biol. 15, 152.

Presgraves DC. 2002. Patterns of postzygotic isolation in Lepidoptera. Evolution 56, 1168–1183.

Pritchard JK, Stephens M, Donnelly P. 2000. Inference of population structure using multilocus genotype data. Genetics 155, 945–959.

Rabosky DL, Talaba AL, Donnellan SC. Lovette IJ. 2009. Molecular evidence for hybridization between two Australian desert skinks, *Ctenotus leonhardii* and *Ctenotus quattuordecimlineatus* (Scindidae: Squamata). Mol. Phylogenet. Evol. 53, 368–377.

Racimo F, Sankararaman S; Nielsen R, Huerta-S Sánchez E. 2015. Evidence for archaic adaptive introgression in humans. Nat. Rev. Genet. 16, 359–371.

Rieseberg LH. 1997. Hybrid origins of plant species. Annu. Rev. Ecol. Syst. 28, 359–389.

Rosanov JM, Vinogradov AE. 1998. Precise DNA cytometry: investigation of individual variability in animal genome size. Tsitol. 40, 792–800.

Roux C, Fraïsse C, Romiguier J, Anciaux Y, Galtier N, Bierne N. 2016. Shedding light on the grey zone of speciation along a continuum of genomic divergence. PLoS Biol. 14, e20000234.

Schmid M, Steinlein C, Bogart JP, Feichtinger W, León P, La Marca E, Díaz LM, Sanz A, Chen S-H, Hedges SB. 2010. Chromosomes of terraranan frogs: Insights into vertebrate cytogenetics. Cytogenet. Genome Res. 130–131, 1–568.

Singhal S, Moritz C. 2013. Reproductive isolation between phylogeographic lineages scales with divergence. Proc R. Soc.B. 280, 20132246.

Shaw KL. 2002. Conflict between nuclear and mitochondrial DNA phylogenies of a recent species radiation: what mtDNA reveals and conceals about modes of speciation in Hawaiian cricket. PNAS 99, 16122–16127.

Skorinov D, Bolshakova DS, Donaire-Barroso D, Pasynkova RA, Litvinchuk S. 2018. Karyotypic analysis of the spined toad, *Bufo spinosus* Daudin, 1803 (Amphibia: Bufonidae). Russ J. Herp. 25, 253–258.

Speybroeck J, Beukema W, Crochet P-A. 2010. A tentative species list of the European herpetofauna (Amphibia and Reptilia) – an update. Zootaxa 2492, 1–27.

Steindachner F. 1867. Reise der österreichischen Fregatte Novara um die Erde in den Jahren 1857, 1858, 1859 unter den Bafehlen des Commodore B. von Wüllerstorf-Urbair. Zologischer Theil. Amphibien, Vienna, Austria.

Stöck M. 1998. Mating call differences between diploid and tetraploid green toads (*Bufo viridis* complex) in Middle Asia. Amphibia-Reptilia 19: 29–42.

Stöck M, Günther R, Böhme W. 2001a. Progress towards a taxonomic revision of the Asian *Bufo viridis* group: Current status of nominal taxa and unsolved problems (Amphibia: Anura: Bufonidae). Zool. Abh. Dres. 51, 253–319.

Stöck M, Frynta D, Grosse WR, Steinlein C, Schmid M. 2001b. A review of the distribution of diploid, triploid and tetraploid green toads (*Bufo viridis* complex) in Asia including new data from Iran and Pakistan. Asiat. Herpetol. Res. 9, 77–100.

Stöck M, Lamatsch DK, Steinlein C, Epplen JT, Grosse W-R, Hock R, Klapperstück T, Lampert KP, Scheer U, Schmid M, Schartl M. 2002. A bisexually reproducing all-triploid vertebrate. Nature Genet. 30, 325–328.

Stöck M, Steinlein C, Lamatsch DK, Schartl M, Schmid M. 2005. Multiple origins of tetraploid taxa in the Eurasian *Bufo viridis* subgroup. Genetica, 124, 255–272.

Stöck M, Moritz C, Hickerson M, Frynta D, Dujsbayeva T, Eremchenko V, Macey JR, Papenfuss TJ, Wake DB. 2006. Evolution of mitochondrial relationships and biogeography of Palearctic green toads (*Bufo viridis* group) with insights in their genome plasticity. Mol. Phylogenet. Evol. 41, 663–689.

Stöck M, Sicilia A, Belfiore NM, Buckley D, Lo Brutto S, Lo Valvo M, Arculeo M. 2008. Post-Messinian evolutionary relationships across the Sicilian channel: Mitochondrial and nuclear markers link a new green toad from Sicily to African relatives. BMC Evol. Biol. 8, 56.

Stöck M, Ustinova J, Lamatsch DK, Schartl M, Perrin N, Moritz C. 2010. A vertebrate reproductive system involving three ploidy levels: hybrid origin of triploids in a contact zone of diploid and tetraploid Palearctic green toads (*Bufo viridis* group). Evolution 64, 944–959.

Stöck M, Savary R, Colliard C, Biollay S, Jourdan H, Perrin N. 2013. Low rates of X-Y recombination, not turnovers, account for homomorphic sex chromosomes in several diploid species of Palearctic green toads (*Bufo viridis* group). J. Evol. Biol. 26 674–682.

Stugren B, Tassoula P. 1987. Uber die wechselkröte (*Bufo viridis* Laur.) aus Zypern. Studia univ. Babes-Bolyai, Biologia XXXII, 2.

Sueur J, Aubin T, Simonis C. 2008. Equipment review: *Seewave*, a free modular tool for sound analysis and synthesis. Bioacoustics 18, 218–226.

Tiffin P, Olson MS, Moyle LC. 2001 Asymmetrical crossing barriers in angiosperms. Proc. R. Soc. B 268, 861–867.

Trochet A, Moulherat S, Calvez O, Stevens VM, Clobert J, Schmeller DS. 2014. A database of life-history traits of European amphibians. Biodivers. Data J. 2, e4123.

Turelli M, Orr HA. 2000 Dominance, epistasis and the genetics of postzygotic isolation. Genetics 154, 1663–1679.

Toews DPL, Brelsford A. 2012. The biogeography of mitochondrial and nuclear discordance in animals. Mol. Ecol. 21, 3907–3930.

Újvari B, Casewell NR, Sunagar K, Arbuckle K, Wüster W, Lo N, O'Meally D, Beckmann C, King GF, Deplazes E, Madsen T. 2015. Widespread convergence in toxin resistance by predictable molecular evolution. PNAS 112, 11911–11916.

Vences M, de Pous P, Nicolas V, Díaz-Rodríguez J, Donaire D, Hugemann K, Hauswaldt JS, Amat F, Barnestein JAM, Bogaerts S, Bouazza A, Carranza S, Galán P, González de la Vega, JP, Joger U, Lansari A, El Mouden EH, Ohler A, Sanuy D, Slimani T, Tejedo M. 2014. New insights on phylogeography and distribution of painted frogs (*Discoglossus*) in northern Africa and the Iberian Peninsula. Amphibia-Reptilia 35, 305–320.

Vinogradov AE, Borkin LJ, Günther R, Rosanov JM. 1990. Genome elimination in diploid and triploid *Rana esculenta* males: cytological evidence from DNA flow cytometry. Genome 33, 619–627.

Vinogradov AE, Borkin LJ. 1993. Allometry of base pair specific-DNA contents in Tetrapoda. Hereditas 118, 155–163.

Warren DL, Glor RE, Turelli M. 2010. ENMTOOLS: a toolbox for comparative studies of environmental niche models. Ecography 33, 607–611.

Watanabe S, Hajima T, Sudo K, Nagashima T, Takemura H, Okajima H, Nozawa T, Kawase H, Abe M, Yokohata T, Ise T, Sato H, Kato E, Takata K, Emori S, Kawamiya M. 2011. MIROC-ESM 2010: model description and basic results of CMIP5-20c3 m experiments. Geosci. Model. Dev. 4, 845–872.

Weisrock DWK, Hozak H, Larson A. 2005. Phylogeographic analysis of mitochondrial gene flow and introgression in the salamander *Plethodon shermani*. Mol. Ecol. 14, 1457–1472

Wetherington J, Kotora K, Vrijenhoek R. 1987. A test of the spontaneous heterosis hypothesis for unisexual vertebrates. Evolution 41, 721–723.

Wielstra B, McCartney-Meslstad E, Arntzen JW, Butlin RK, Shaffer HB. 2019. Phylogenomics of the adaptive radiation of *Triturus* newts supports gradual ecological niche expansion towards an incrementally aquatic lifestyle. Mol. Phylogenet. Evol. 133, 120–127.

Willis SC, Farias IP, Ortí G. 2014. Testing mitochondrial capture and deep coalescence in Amazonian cichlid fishes (Cichlidae: *Cichla*). Evolution 68, 256–268.

Yakovlev VA. 1987. Dispersal of the marsh frog in Altay. Pp. 100-101 in Irisov EA (Ed). Threatened, Rare and Poorly Studied Plants and Animals of Altayskiy Kray and Problems of Their Conservation. Barnaul, Russia.

Zieliński P, Nadachowska-Brzyska K, Wielstra B, Szkotak R, Covaciu-Marcov SD, Cogălniceanu D, Babik W. 2013. No evidence for nuclear introgression despite complete mtDNA replacement in the Carpathian newt (*Lissotriton montandoni*). Mol. Ecol. 22, 1884–1903.

Zinenko O, Sovic M, Joger U, Gibbs HL. 2016. Hybrid origin of European Vipers (*Vipera magnifica* and *Vipera orlovi*) from the Caucasus determined using genomic scale DNA markers. BMC Evol. Biol. 16, 76.

Zink RM, Barrowclough G. 2008. Mitochondrial DNA under siege in avian phylogeography. Mol. Ecol. 17, 2107–2121.